BIO-INSPIRED LOW-COST ROBOTIC JOINT WITH REDUCED LEVEL OF BACKLASH AND A NOVEL APPROACH: THE EMULATED ELASTIC ACTUATOR

József Veres

Faculty of Information Technology

Pázmány Péter Catholic University

Scientific adviser:

György Cserey, Ph.D.

A thesis submitted for the degree of

Doctor of Philosophy (Ph.D)

2013

I would like to dedicate this thesis to my loving family ...

Acknowledgements

List of Figures

List of Tables

Summary of Abbreviations

Abbreviation	Concept
PMSM	Permanent Magnet Stepper Motor
HSM	Hybrid Stepper Motor
SEA	Series Elastic Actuator
VSA	Variable Stiffness Actuator
FIR	Finite Impulse Response
DAC	Digital to Analog Converter
ADC	Analog to Digital Converter
SPI	Serial Peripheral Interface
PC	Personal Computer
DOF	Degree Of Freedom
PCB	Printed Circuit Board
LUT	Look Up Table
MSB	Most Significant Bit
LSB	Least Significant Bit
CAD	Computer Aided Design

Abbreviation	Concept
PWM	Pulse Width Modulation
COM	Center Of Mass
EOM	Equation of Motion
CPR	Counts Per Revolution
GRF	Ground Reaction Force
EMI	ElectroMagnetic Interference

Contents

Chapter 1

Introduction

1.1 Motivations

Walking on two legs, or bipedalism, is the capability of just a few species on the globe. Strictly speaking, only the primates are able to walk like us. Even for a human takes years to acquire the ability of stable walking. Thus, not surprisingly, the area of biped walking robots is one of the most researched fields of robotics.

For almost the whole 20th century, creating biped robots that feature balancing was a very difficult task to accomplish. As a result, robotic locomotion were mainly limited to wheeled or multi-legged solutions. After the first revolution of electronics, that introduced the mass of cheap microprocessors, building of a two-legged robot that maintains its postural stability became feasible. During that period of time, Japan had almost no competitor. Researchers at Waseda University [1] are thought as the pioneers of biped walking robots. In 1986, Honda Inc. started a large-scale research on biped robots to construct and commercialize full-size humanoid robots. The goal was to create human-like robots that would be capable of assisting elderly, or performing tasks that are dangerous to humans. After fifteen years of extensive research, whereof the first seven prototypes out of ten had only legs without upper body, ASIMO [2] the most famous humanoid walking robot has been introduced. The child-size robot could walk, run, turn, climb stairs, grasp objects and interact with its environment. Despite all the success, the vision of biped robots assisting us, has still not yet been achieved. One of the reasons for that is the lack of appropriate actuation mechanism that prevents us to successfully mimic the human locomotion in everyday situations. In this dissertation I will attempt to face that issue of biped walking robots.

1.2 Biped robots

Biped robots is a subclass of legged robots. Since, a complete humanoid robot must have two legs, therefore all humanoid robots can be thought as biped robots. However, a biped robot do not necessarily have arms and head. Strictly speaking, a biped is an open kinematic chain with two sub-chains that are the legs. In almost all the cases, there is an extra sub-chain connected to the center point of the hip, the torso that mimics the upper body.

Fig. 1.1 illustrates the single support phase where only one leg touches the ground at a time. The leg that is in contact with the ground called the stance leg and the other one is the swing leg. In this phase the robot is underactuated

11
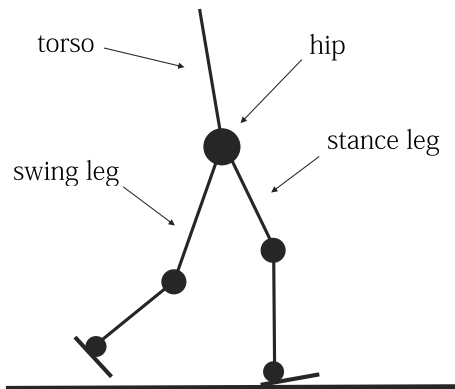
Figure 1.1: Biped robot (single support phase)

since there is no direct control over the tipping. Similarly, there is the double support phase where both legs are in contact with the ground and the robot is overactuated.

Walking can be thought as the alternating phases of single and double support. The difference between running and walking is the presence of flight phase where both legs are in the air for a short period. To simplify the non-trivial problem of walking often planar bipeds are used that, in contrast to the full three-dimensional ones, can only move in the sagittal plane.

The simplest gait is the statically stable gait where the robot's center of mass (COM) is always within the support polygon of the feet. That means, at any point of the gait the robot could be stopped and it does not tip over. In contrast, there is dynamically stable gait. Despite the fact that it produces a stable walking while the robot is in motion, the gait could not be stopped at any time without the risk of tipping over. The reason for that is the dynamically stable gait allows the biped's center of pressure (CoP) to be on the boundary of the support polygon [3]. Strictly speaking, in this case CoP is the point on the ground where the resultant of the ground-reaction force acts. In the literature of this field the term of the Zero Moment Point (ZMP) is often used instead of the CoP. The criterion of ZMP was originally defined by Vukobratovic *et al.* in 1972 and become the most widely used method to control the bipeds locomotion to be always dynamically stable [4].

It is important to note that, however, the ZMP criterion is an effective and rel-

atively easily be implemented technique, it features extremely low energy efficiency compared to human walkers. The main reason for that is the high feedback gains required to maintain local stability. The high feedback gains often cause unwanted active braking of the actuators resulting unnecessary negative work. Furthermore, it requires good power transmission to avoid oscillation, that increase the cost of the robot.

In addition to the statically and dynamically stable walking, there is a relatively new approach, the limit cycle walking [5]. The limit cycle walking could be defined as a normally periodic sequence of steps that is globally stable but not locally stable at all the time. Normally periodic sequence of steps means that the required walking is the exactly same closed trajectory repeating in state space. In contrast to the conventional trajectory control, where all the points on the trajectory needs to attract their local neighborhood in the state space, in this case it can be relaxed. The reason for that is the neighboring trajectories can approach the nominal trajectory over multiple steps. This is often called the cyclic stability.

Unfortunately, the detailed description of the gait synthesis is beyond the scope of the dissertation.

There are three major challenges associated with biped robots [6]. The first one is the limb coordination. Obviously, the ultimate goal of walking is to move the COM of the biped robot from point A to point B that is a low degree of freedom (DOF) task. Since these robots are having high DOF, it can be easily seen that the task of walking does not uniquely specify how the coordination of the limbs must be done. From the many solution, finding one can be a challenge, especially finding the optimum.

The second one is the hybrid dynamics. At the end of the swing or single support phases there are always impacts occur at the instance of the touch down. According to this, the model must have multiple phases that means the model is hybrid. The control of hybrid systems is challenging.

The third difficulty is the underactuation. In contrast to the industrial manipulators, that are fixed to the ground and fully actuated, legged robots are usually underactuated. It means, there are DOFs of the system that cannot be directly controlled. Non-direct control of an underactuated system (for example through inertial coupling) is hard to achieve.

1.3   Goals of the dissertation

Research on biped robots is important for two reasons. On one hand to create walking robots that are able to assist the humanity. For example, in case of a catastrophe of a nuclear plant, that unfortunately lately happened at Japan's Fukushima Daiich, biped robot could be deployed to save human lives. On the other hand, research on biped robots could help us to better understand human locomotion disorders, for example locomotor rehabilitation for individuals with stroke, or how to improve lower-limb prostheses.

High-end humanoid biped platforms are extremely expensive. There are a few low-end commercially available two-legged robots, like the NAO from the Aldebaran Robotics, that are used in academic research. These robots are usually incorporating robotic joints made of standard parts. In terms of actuators, fabrication inaccuracy introduces significant mechanical backlash which is a hard-nonliearity from the control point of view.

Therefore, during my early research I tried to address the issue of non-linearities in the actuators of biped robots by attempting to create a bio-inspired low-cost robotic joint using PMSMs and low-level active control.

In addition to nonlinear phenomena, walking inherently implies dynamics that are not necessarily been addressed by the theory of classical robotics. In contrast to the industrial robots, walking, running or climbing stairs with a two-legged robot requires substantially different approaches.

A new field of robotics is emerging namely the *dynamic walking.* In 2006, a new international conference has established to allow researchers all over the world to share their findings. The central issues are the energy efficiency, dynamic stability and complaint actuation. Compliance is turned to be essential for the fundamental interaction with the environment. During the half-year, while I had the privilege to get involved in the research of James Schmiedeler's group at the Locomotion And Biomechanics Laboratory (Notre Dame), I understood the limits of the principles of classical robotics. After my returning to Hungary, I started to work on a novel concept that could improve the dynamics of biped robots.

Thus, during my late research I tried to investigate a new type of robotic actuator that can emulate the different kind of elasticity under software control or in other words, to be able to implement intrinsic compliance that is found to be crucial for dynamic movements.

With this new concept, unlike existing mechanical solutions, like SEA [7] that are limited to fixed elastic behaviour, change in the parameters of the elasticity could become available on the fly. Considering the fact that the springiness would being emulated in software, exotic non-linear functions would become realizable.

1.4   Framework of the dissertation

In Chapter 2, a bio-inspired low-cost robotic joint is proposed that is based on PMSMs. The ability of reduction in the level of backlash under active control is investigated. The numerical results acquired through simulations, and experiments are discussed and then compared to the standard robotic joint configuration.

In Chapter 3, a novel concept is introduced namely the software controlled emulation of physical elasticity of a robotic joint. Not only the concept, but also the hardware implementation is presented along with simulations and experiments that support the functionality of the actuator.

In Chapter 4, the methods and the new scientific results of the dissertation are summarized. Finally, the possible applications are highlighted.

Chapter 2

Bio-Inspired Low-Cost Robotic Joint with Reduced Level of Backlash

Nomenclature

b Measure of a backlash as a distance [m]

β Measure of a backlash as an angle [rad]

r Radius of a gear [m]

τ Torque [Nm]

i Current [A]

I Nominal current [A]

θ Angle [rad]

J Inertia [kg m^2]

B Viscous friction [Nms/rad]

F Force [N]

ω Angular velocity [rad/s]

n Gear ratio

N Pole number

x Linear position [m]

k Feedback strength [1/s]

K Stiffness [N/m]

e Angle difference [rad]

E Angle difference treshold [rad]

T Time period [s]

Subscripts

m Motor

a,b Phase a and b

p Pole

g Intermediate gear

l Load (real)

L Load (estimated)

r Reaction

d Desired

c Computed

t Total

j Index of the elements in pair (1,2)

2.1 Introduction

Most robotic joints are actuated by rotational mechanisms. Typically, these mechanisms are driven by electric motors whose operating speed is higher than what the joints actually require. Gearboxes are then used to reduce the speed of the joints and also to increase their torque. The incorporation of a gearbox corrupts the continuity of the torque transmission in most cases because of the backlash phenomenon. Backlash originates from the gear play that results from the imperfectness of the fabrication or the increased wear level of the mating gears. During static motion this introduces only positioning errors but in dynamic cases limit-cycles may occur. Some mechanical and control solutions that reduce the effect of backlash are given below.

Starting with the control solutions it can be concluded that numerous publications are available in the field. Most of these papers offer solutions for the modeling and identification of the mechanical system together with the backlash phenomenon [8, 9, 10, 11, 12, 13]. Different approaches include vibration analysis [14], wavelet analysis [15], utilizing fuzzy logic [16] and Kalman filters [17]. Compensation of the effect of the backlash using Stribeck friction was reported in [18] and [19]. Controllers and adaptive controllers for mechanical systems with backlash can be found in [20, 21, 22]. There are papers focusing on different applications like positioning [23] or target tracking [24]. Hovland *et al.* [25] showed a backlash identification in robot transmission. Backlash compensation for a humanoid robot with a disturbance observer [26], as well as with a genetic algorithm [27], were reported. Turning now to mechanical solutions, a few examples include anti-backlash gears, pre-loaded gears, and harmonic drives. The latter were originally developed for aerospace and military applications and offer a very low level of backlash with high reduction ratios in a compact size. These advantages have made the harmonic drive the most widely used robotic gear type. The disadvantages of using this type of mechanical solution are its increased level of elasticity and its significantly higher cost.

The cost of the actuator can be an issue, for example in the cases where high degree of freedom (DOF) robots are needed. Good examples for this issue are the humanoid or biped robots where tens of joints are usually required to be actuated. In almost all cases these are series manipulators. According to Akhter *et al.* [28] a large percent of these robots are not equipped with harmonic drives but use standard gears presumably to be more cost effective but at the same time suffering

from the effect of backlash.

In this chapter, a low-cost alternative solution for decreasing the effect of backlash in robotic joints will be presented. The proposed solution reduces backlash by incorporating a flexor-extensor pair of low-cost PM stepper motors bundled with low-end integrated gearboxes. The method was inspired by the biological structure of human limbs, which inspiration will be briefly introduced in the following section.

There are related studies in the literature. For parallel manipulators Sven *et al.* [29] and Boudreau *et al.* [30] have recently published their dual motor mechanism that can be used to reduce the level of backlash. The original level was reported to be reduced by over 90%. Turning to the series manipulators, which is only in the scope of this work, Kiyoshi *et al.* [31, 32] presented their twin-drive mechanism that is related to the solution of this work. They were using direct-drive DC motors, which creates a significant limitation since without gears the robots that are in the scope of this work could not be built due to the lack of the adequate torque capability.

It has to be emphasized that this approach does not target the area of the classical industrial manipulators — where precision and repeatability are more important than the cost of the actuators — but the robots with high DOF that require negligible backlash at low-cost.

2.2 The inspiring human flexor-extensor mechanism

Human muscles can only exert force in one direction. This is why it is always necessary to have counterparts to be able to create repetitive motion with the help of cyclic contractions, like walking. These muscle groups are called the agonists and the antagonists. Well known examples are the biceps brachii and triceps brachii muscles of the upper arm. By using these antagonistic pairs we are able to perform a wide variety of motions. For example, if the two antagonistic muscles are contracted simultaneously, it is possible to change the stiffness of the joint. In terms of precise co-ordination of these muscle groups, complex neural controls are generally required. However, simple reflex-arcs exist that can realize fast but very simple reactions. A good example for that is the collateral inhibition of the antagonistic muscles that serves as a basic mechanism of muscle co-operation. This

idea inspired me to design and implement an alternative solution for the backlash problem of low-cost robotic joints.

My approach is to use a pair of low-cost actuators instead of a more expensive solution that contains a harmonic drive. Then one actuator will be dedicated for the right turn and the other for the left turn like flexing and extending in the human limbs. A smooth motion can be realized with a proper control by mimicking a simple reciprocal innervation of the two muscle groups. The main advantage of this approach is that the backlash of the joint can be almost completely eliminated with a simple digital control that is implemented using a low-end microcontroller.

2.3 Description of the proposed robotic joint

As it was introduced in the previous sections this approach uses a pair of actuators. These include gearboxes with a significant level of backlash. Fig. 2.1 shows the structure of the proposed joint. The two actuators that are facing in an opposite direction are attached to a fixed body (Link 1). The outputs of the gearbox axes are directly coupled with the output of the robotic joint that is actuated (Link 2). The following convention will be used: Motor 1 is assigned to the right turn (flexing) and Motor 2 for the left turn (extending). This could be arbitrarily set but the above written convention will be used. The gearboxes are low-end spur type and are integrated with the PM stepper motors. These are three stage gearboxes with a gear reduction ratio of 100:1 ($n_1 = n_2 = 10$). The total backlash (β_t) of the individual gearboxes is 0.0192 rad. Nowadays the permanent magnet stepper motors are becoming affordable and widely used not only in the industry but even in the field of aerospace engineering[33]. These motors or the hybrid types combined with a simple microcontroller can perform well [34, 35, 36, 37] even in the low speed region.

In order to actuate the joint, low-cost, two-phase, bipolar permanent magnet stepper motors were chosen. Each of these has six pole-pairs with $8\,\Omega$ coil resistance and 24 mH coil inductance. The nominal currents are 0.45 A with holding torques of 0.012 Nm. The inertia of the rotors are $1.5 \times 10^{-6}\ \mathrm{kg\,m^2}$ with motor constants of 0.004 Nm/A. Both motors are equipped with on-axis rotary encoders. Non-contacting sensor is the type that is the most widely used nowadays since these are less prone to wear out. Optical encoders are used as standards but recently the magnetic type rotary encoders are getting to become a good alternative solution. The latter one offers a cost effective way of angular measurement at the price of

20
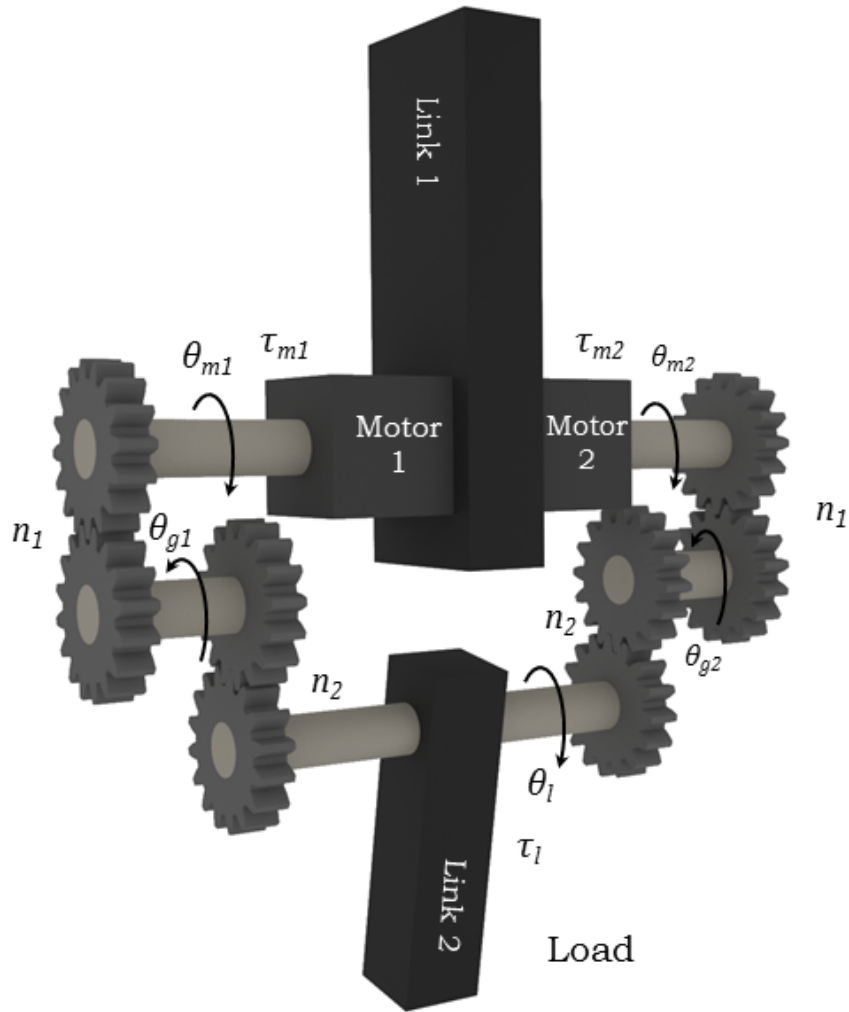
Figure 2.1: Electromechanical model.

the decreased maximal spatial resolution. In this work AS5045 type sensors are used that provide 12 bit absolute resolution. This is equivalent to a 4096 CPR that is acceptable for these robots. The sampling rate of the sensor is 10.4 kHz. Besides the two sensors that measure the angular position of the two motors, one more sensor is used. It is optional, but the reason why it is used here is to assist the verification of the backlash reduction.

The implemented prototype is shown in Fig. 2.2. The two PM stepper motors are denoted by (A) and the corresponding gearboxes by (B). On the top of the motors (C) denotes the magnetic encoders and the driving circuits. A3979 is
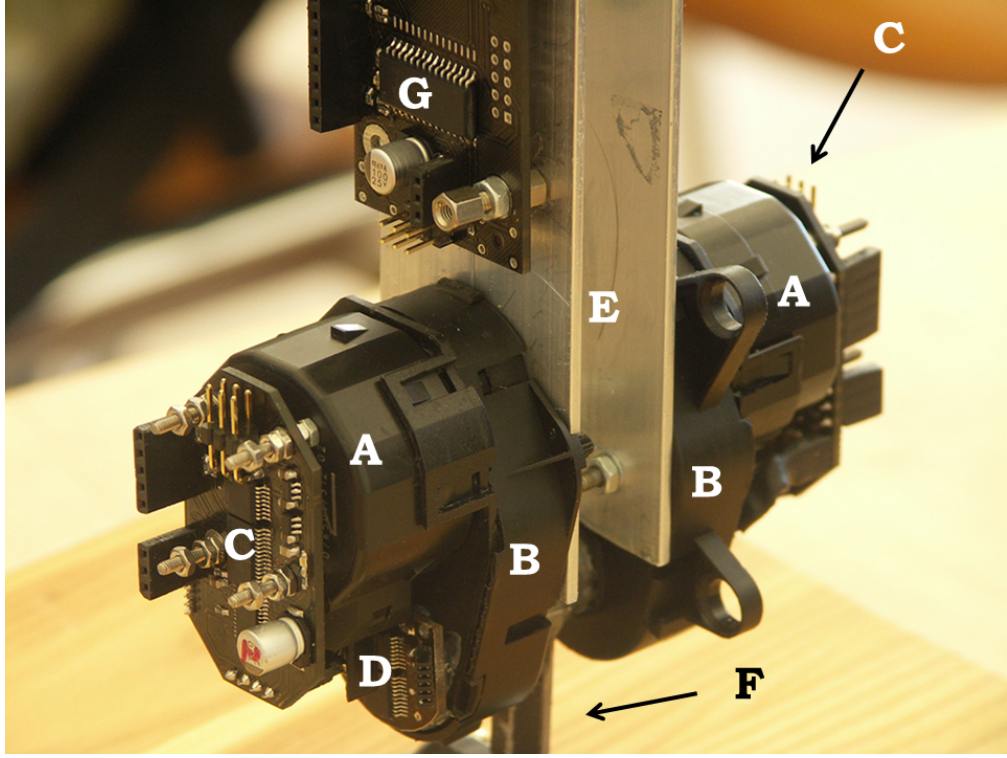
Figure 2.2: Photo of the implemented prototype.

used as a motor driver along with a PIC24HJ12GP202 16bit microcontroller. The driver features internal PWM current control which reference value is updated by the microcontroller. (D) marks the optional load side encoder that measures the angular position of Link 2 respective to Link 1. The letters (E) and (F) indicate Link 1 and Link 2 respectively. The full motion control algorithm is implemented onboard that means a PIC24FJ16GA002 microcontroller responsible for the complete digital control (G). Personal computer is used only for data acquisition.

2.4 Modeling of the joint

2.4.1 Stepper motor model

The instantaneous torque of the permanent magnet stepper motor can be written as [38]

$$\tau = -K_m \left[i_a \sin \left(N_r \theta \right) - i_b \cos \left(N_r \theta \right) \right], \qquad (2.1)$$

where K_m (Nm/A) is the motor constant, i_a (A) is the current in phase a, i_b (A) is the current in phase b, N_r is the number of the rotor poles, and θ (rad) is the

2. BIO-INSPIRED LOW-COST ROBOTIC JOINT WITH REDUCED LEVEL OF BACKLASH
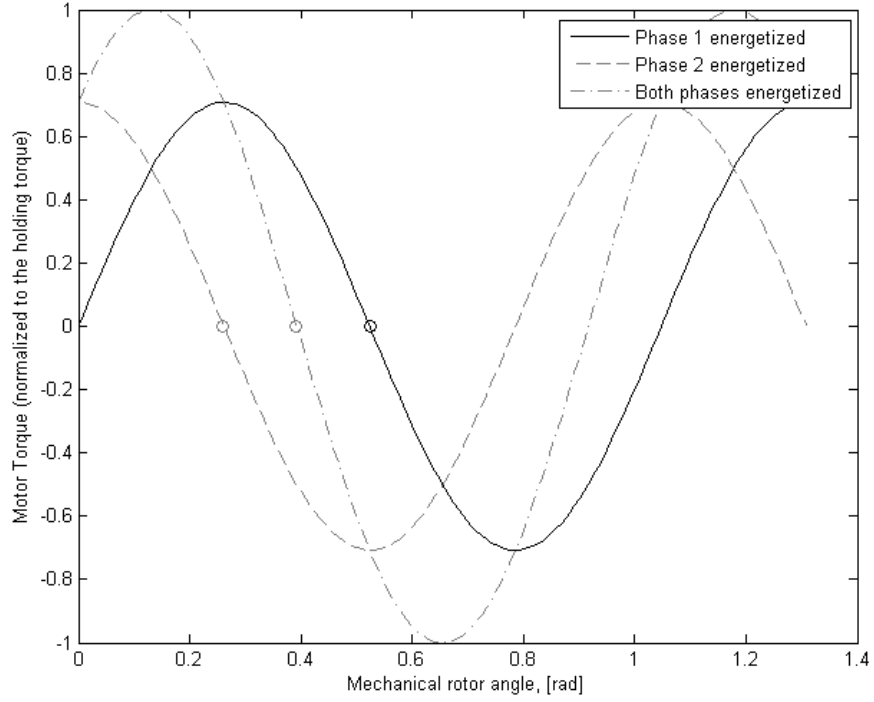
Figure 2.3: Normalized static torque characteristic of the stepper motor.

mechanical angle of the rotor.

Fig. 2.3 shows this static torque characteristic. It is modeled as a sinusoid-like function of the rotor's angular position where the higher harmonics like the 4th harmonic (the cogging torque) are neglected. Both the one-phase and the two-phase excitations are plotted (the latter two-phase excitation was chosen since it offers more torque). The static torque is normalized and the stable points (o), that represent the rotor's rest position if no external load applied, are marked.

Then the differential equation of the motor's dynamic is given by

$$\frac{\mathrm{d}^2\theta}{\mathrm{d}t^2} = \frac{-K_m i_a \sin\left(N_r\theta\right) + K_m i_b \cos\left(N_r\theta\right) - B\omega}{J} \tag{2.2}$$

where ω (rad/s) is the mechanical angular velocity, B $(\mathrm{N\,m\,s/rad})$ is the viscous friction coefficient and J $(\mathrm{Kg\,m}^2)$ is the inertia of the rotor.

The coils are excited with full-stepping method that can be written up in the

23
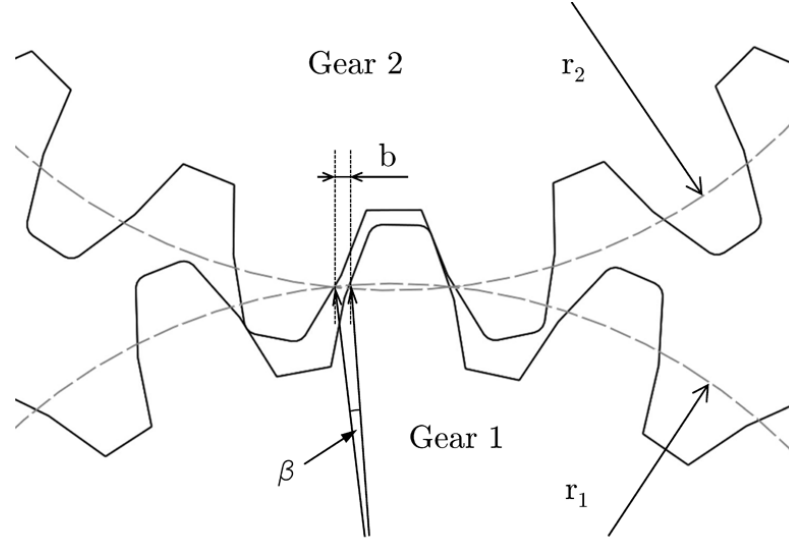
Figure 2.4: Illustration of the backlash

following way

$$i_a = I \sin (N_r \theta_d) \tag{2.3}$$

$$i_b = I \cos (N_r \theta_d), \tag{2.4}$$

where I (A) is the nominal current of the motors' coil and θ_d is the desired angle where $\theta_d \in \left[\frac{\pi}{4}, \frac{3\pi}{4}, \frac{5\pi}{4}, \frac{7\pi}{4} \right]$.

2.4.2 Gear train and backlash model

First assume that the transmission of the motors is free of backlash and all the elastic deformations are neglected. In this case the angular position of the load can be written in the following forms

$$\theta_l = \frac{\theta_{m1}}{n_1 n_2} = \frac{\theta_{g1}}{n_2} = \frac{\theta_{m2}}{n_1 n_2} = \frac{\theta_{g2}}{n_2}, \tag{2.5}$$

where n_1 is the reduction ratio between the first and the second stage and n_2 is between the second and the last stage. This linear formula turns to be highly non-linear once the effect of the backlash is added. Two different scenarios are usually distinguished. Contact Mode (CM) when the two mating gears are in contact and the Backlash Mode (BM) when these are disengaged [20]. Fig. 2.4 shows a gearplay between mating gears. The value of the backlash measured as a linear distance is
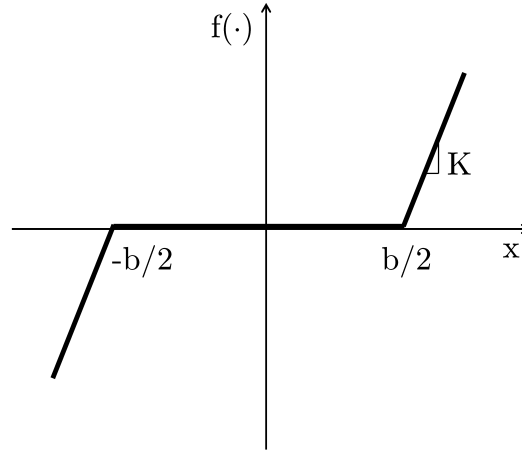
Figure 2.5:   Piecewise linear function for backlash modelling.

denoted by b. It can be approximated by using the angle β (rad) and the radius r_1 as

$$b \approx \beta r_1, \tag{2.6}$$

since β is a small angle. Similarly it is equal to the radius of Gear 2 multiplied by the angle of backlash measured on the second gear. In the literature there are different approaches to model the effect of the backlash [11, 12, 17, 22]. One of these is the contact model type that is using non-linear reaction forces [21]. The idea is to model the occurring contact between the mating gears with a non-linear elastic force that depends on the relative position (x) of the mating gears. The starting point $(x = 0)$ is when the gears are at the center of the empty space. The relative position of the mating gears is defined as

$$x = r_1\theta_1 - r_2\theta_2. \tag{2.7}$$

For simplicity, a piecewise linear function is used to express the reaction forces, that can be seen in Fig. 2.5.

$$f(x) = \begin{cases} K(x + b/2) & x < -b/2 \\ 0 & |x| \leq b/2 \\ K(x - b/2) & x > b/2 \end{cases} \tag{2.8}$$

The stiffness K and individual backlash b values are expected to be identical for all the stages of the gear trains. The numerical values are approximated by

experimental results that are presented in Section 2.6. By using (2.7) the reaction force acting on the teeth of Gear 1 can be defined as

$$F_r = f(r_1\theta_1 - r_2\theta_2), \tag{2.9}$$

and the torques of Gears 1 and 2, created by the reaction forces acting on the mating teeth are given by

$$\tau_1 = F_r r_1 \tag{2.10}$$

$$\tau_2 = -F_r r_2. \tag{2.11}$$

2.4.3 Complete model

The complete electromechanical model of the proposed joint is approximated as a five-inertia system that includes backlash and viscous friction. According to the naming conventions of Fig. 2.1, the index of m refers to the motor number and the first stage of the gearbox, g to the second stage, and l to the load and the last stage. Then by using (2.2), (2.6) and (2.9) the complete model becomes

$$\frac{\mathrm{d}^2\theta_{m_j}}{\mathrm{d}t^2} = \frac{\tau_{m_j} - B_m\omega_{m_j} - F_{mg_j}r_m}{J_m} \tag{2.12}$$

$$\frac{\mathrm{d}^2\theta_{g_j}}{\mathrm{d}t^2} = \frac{-B_g\omega_{g_j} + F_{mg_j}r_{gm} - F_{gl_j}r_{gl}}{J_g} \tag{2.13}$$

$$\frac{\mathrm{d}^2\theta_l}{\mathrm{d}t^2} = \frac{\tau_l - B_l\omega_l + (F_{gl_1} + F_{gl_2})r_l}{J_l} \tag{2.14}$$

$$\tau_{m_j} = -K_m \left[i_{a_j} \sin\left(N_r\theta_{m_j}\right) - i_{b_j} \cos\left(N_r\theta_{m_j}\right) \right] \tag{2.15}$$

$$i_{a_j} = I \sin\left(N_r\theta_{d_j}\right) \tag{2.16}$$

$$i_{b_j} = I \cos\left(N_r\theta_{d_j}\right) \tag{2.17}$$

$$F_{mg_j} = f(\theta_{m_j}r_m - \theta_{g_j}r_g) \tag{2.18}$$

$$F_{gl_j} = f(\theta_{g_j}r_g - \theta_l r_l), \tag{2.19}$$

where j, that can be 1 or 2, denotes the element of the actuator pair. The B coefficients are the viscous damping coefficients and τ_l represents all the external forces acting on the load. J_m denotes the combined inertia of the motors and the first stage. J_g is the inertia of the intermediate stage and J_l indicates the inertia of

the load and the last stages. The numerical values were numerically computed on the available CAD drawings of the parts. The forces F_{mg_j} are the reaction forces acting on the mating gears of the first stage ($_m$) and the intermediate stage ($_g$), and similarly F_{gl_j} is the reaction force of the intermediate and the last stage ($_l$).

2.5   Motion control

The control input to the system is the angular velocity reference (ω_{ref}) of the joint. As a first assumption this specifies the rate of change of the desired positions of the two motors. Therefore, the desired angular velocities of the motors are given by

$$\omega_{d_1} = \omega_{ref} \tag{2.20}$$

$$\omega_{d_2} = -\omega_{ref}. \tag{2.21}$$

An open-loop commutation scheme could enforce the desired angular velocity command if proper acceleration and deceleration phases were added in order to prevent the loss of synchronism. That would imply the commonly used trapezoidal speed profile. Unfortunately even that could not guarantee the synchronism in the presence of unknown external loads, therefore closed-loop commutation is used.

In order to keep the commutation synchronised with the rotor, error variables (2.22) are introduced

$$e_j = \theta_{m_j} - \theta_{d_j}. \tag{2.22}$$

Fig. 2.6 shows the flowchart of the two individual motor commutation. In case of an open-loop commutation steps are issued with the necessary delay to achieve the required angular speed. By integrating the issued steps the desired angular position can be achieved (θ_{d_j}). It can be easily seen that once the motor is not able to realize any of the required steps there will be an error (2.22) . In order to prevent the loss of synchronism, if the error is greater than a predetermined threshold (E=0.2 rad), the step must not be issued until the error falls below the threshold.

The closed-loop commutations of the stepper motors are just the low-level parts of the whole motion control. The high-level part is responsible for the generation of the commanded angular velocities (ω_{cmd_j}). The block diagram of the complete

2. BIO-INSPIRED LOW-COST ROBOTIC JOINT WITH REDUCED LEVEL OF BACKLASH

motion control can be seen in Fig. 2.7. In order to reduce the level of backlash a cross-connected feedback is taken. β_d is the desired level of angle difference and it is defined as

$$\beta_d \quad = \quad b_t r_m = \beta_t n_1 n_2, \qquad (2.23)$$

where b_t is the total backlash of the gearbox given as a linear distance, β_t is the angle of the total backlash expressed at the last stage and k is a constant that sets the strength of the error feedback. As it can be seen in Fig. 2.7 the control tries to drive the actuators on the two sides (flexor and extensor) in a way to make $\beta_d - (\theta_{m_1} - \theta_{m_2})$ approach zero. The closer it drives to zero the less the resulting backlash will be. Then the position of the load can be approximated by

$$\theta_l \approx \frac{\theta_{m_1} + \theta_{m_2}}{2 n_1 n_2} = \theta_L. \qquad (2.24)$$

Since θ_l is also measured the comparison of the two trajectories become a good benchmark for the operation of the system.
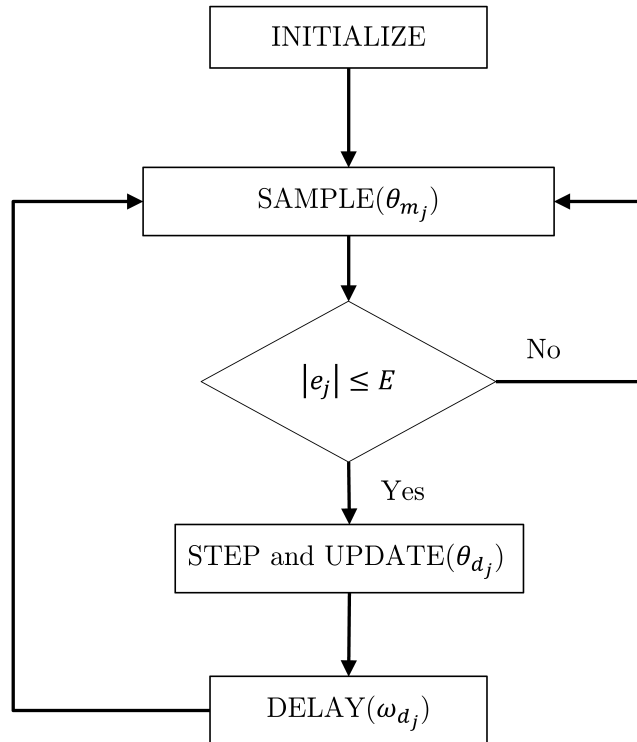
Figure 2.6: Flowchart of the closed-loop commutation.

28
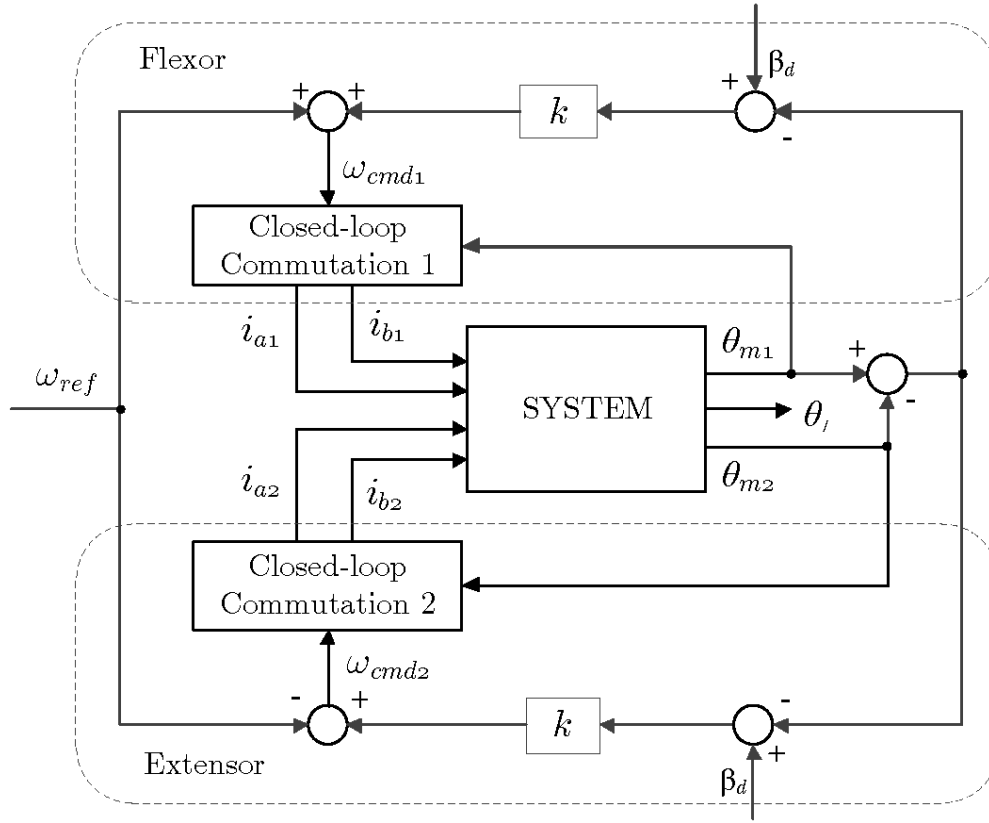
Figure 2.7: Block diagram of the motion control of the joint.

2.6 Simulation and experimental results

For running the simulations MATLAB 8 was used with the help of the built-in numerical differential equation solver that is based on the variable step Runge-Kutta method.

In order to create a basis for comparison a new system is introduced. If one of the flexing-extending actuator pair is removed, a standard robotic joint would be achieved. Let the actuator denoted by index $j = 2$ be omitted, which means the motor and the gears are physically removed. The corresponding complete model will be the same as was derived previously but j is limited to one and F_{gl_2} is set to be zero. In the following, it will be referred to as the *standard case* and the original one as the *flexor-extensor case*.

Fig. 2.8(a) and Fig. 2.8(b) illustrate two of the model validation results where the standard case was used. Both figures show the measured and simulated θ_l load positions as two different τ_l external load torques were applied at about $t = 0.6s$.

29

2.   BIO-INSPIRED LOW-COST ROBOTIC JOINT WITH REDUCED LEVEL OF BACKLASH
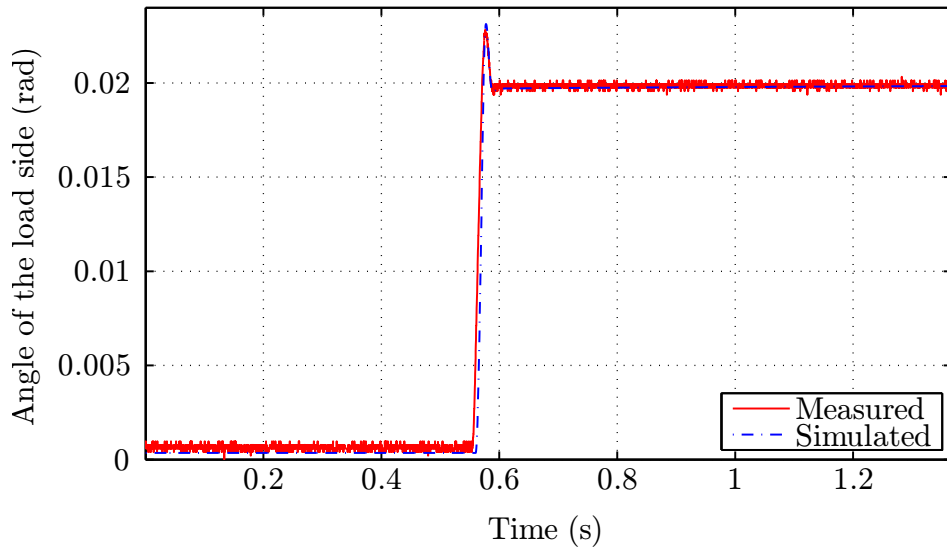
(a) 0.5 Nm
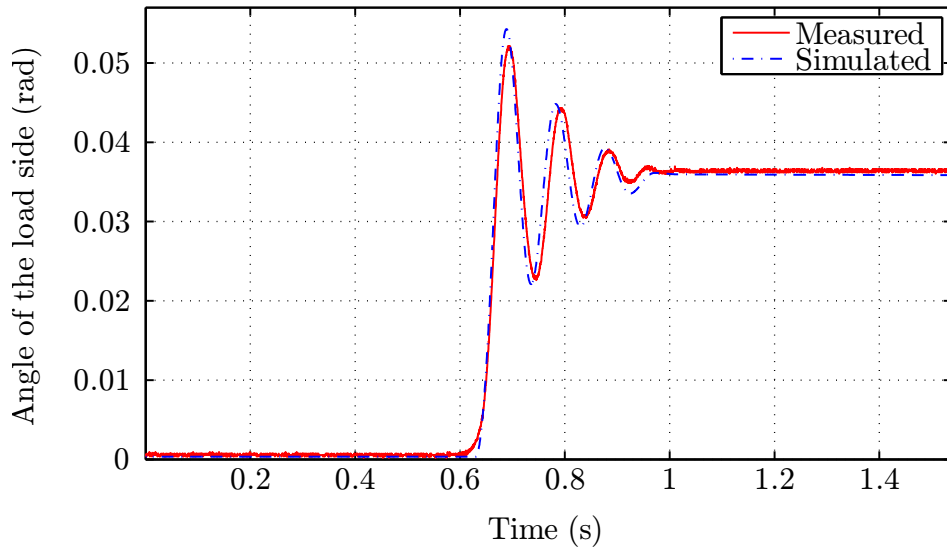
(b) 1.5 Nm

Figure 2.8:   Results of the model validation.

The motors were excited with the maximum constant current in order to produce the maximum holding torque, that prevented the applied external torque to back-drive the motor. The position of the load was set to one extremum of the empty space created by the gearplay.

Then the applied external torque forced the load to move towards the other extremum. The smaller 0.5 Nm torque created a small overshoot that corresponds to the impact of the mating gears. The load position after the impact is just slightly bigger than the original backlash of the gearbox. The larger external torque caused
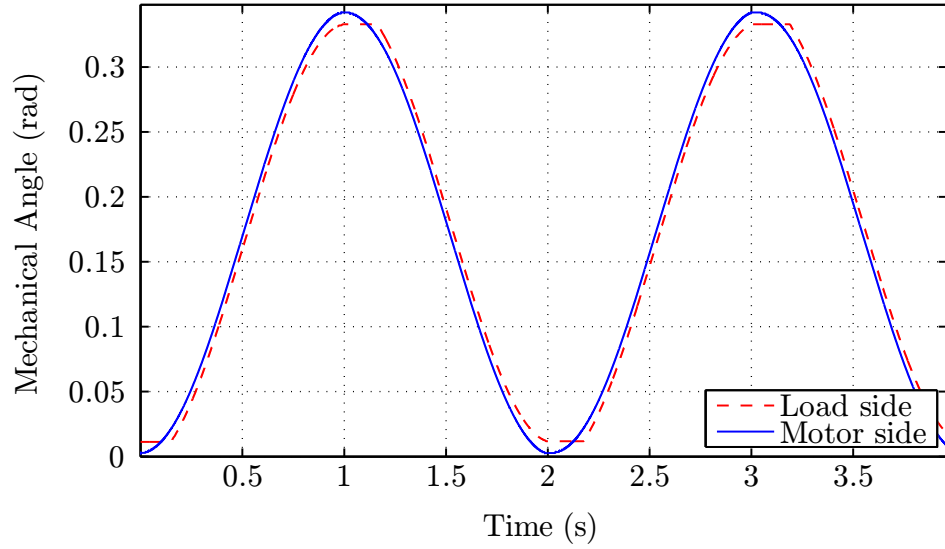
(a) Standard case - Simulation
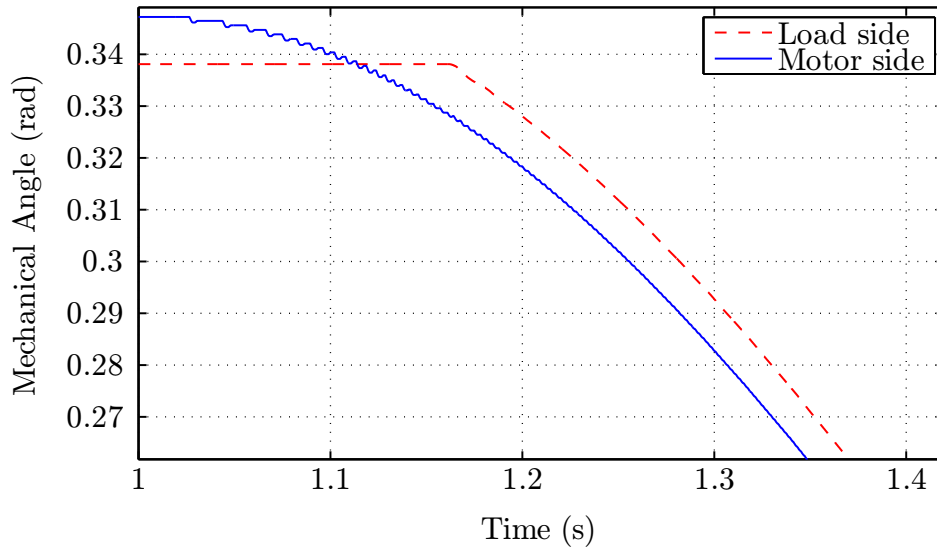
(b) Zoom at the simulation

Figure 2.9: Simulation results of the standard case.

a bigger impact and showed a damped oscillatory motion with a settled position equal to almost the twice of the original backlash.

Figs. 2.9(a)-2.12(b) show the comparison of the new flexor-extensor approach with the standard approach. In both cases the same sinusoidal angular velocity reference (ω_{ref}) was given. Fig. 2.9(a) shows the simulation results of the measured (θ_l) and approximated (θ_L) position of the load. Since there is no external disturbance the position of the load follows the position of the motors with a small difference. The difference between the two curves is enlarged in Fig. 2.9(b). As the
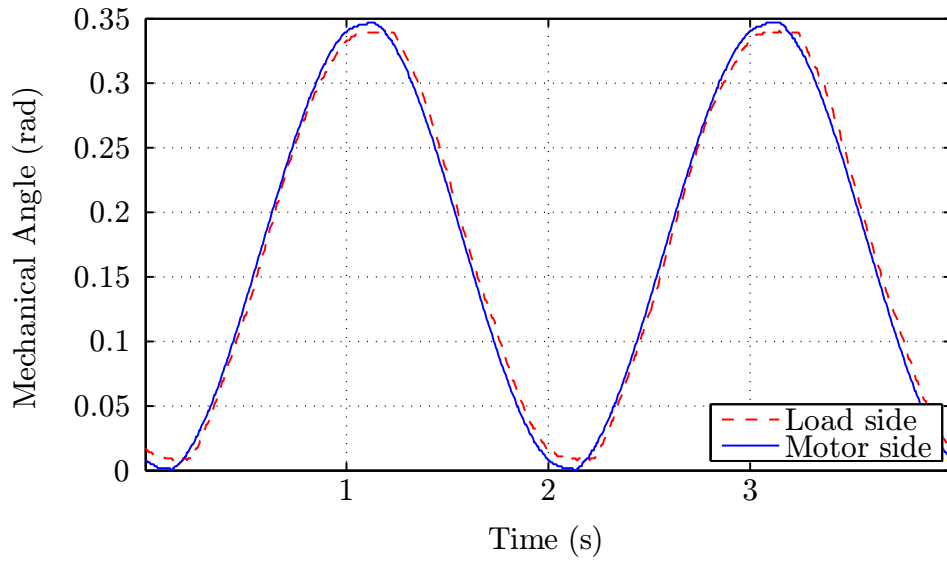
(a) Standard case - Experiment
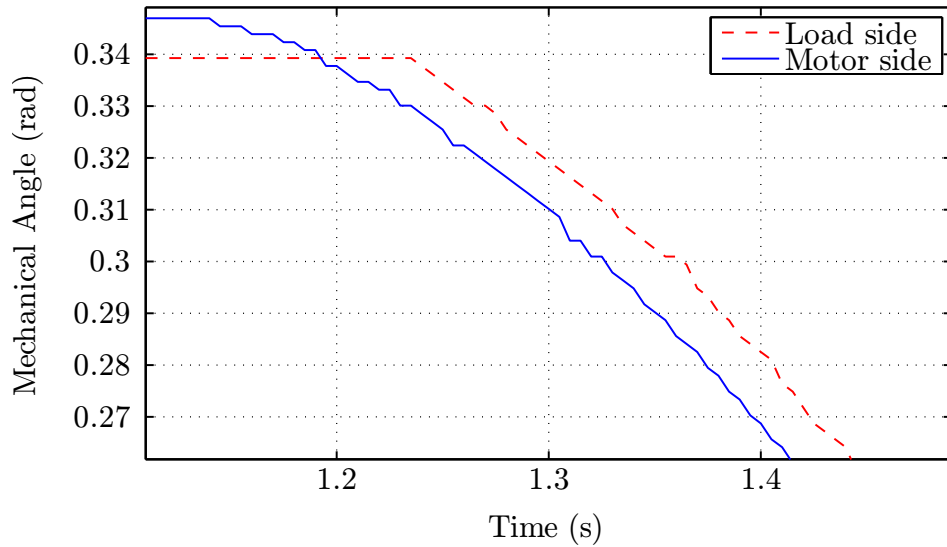
(b) Zoom at the experiment

Figure 2.10: Experimental results of the standard case.

motion of the motors change direction the mating gears smoothly travel the empty space caused by the backlash. First it creates positional inaccuracy and furthermore in the presence of external disturbances (e.g.: caused by other joints) it can create high impacts that has been shown in Fig. 2.8(b). The real measurement is showed in Fig 2.10(a) and the zoomed counterpart in Fig. 2.10(b). The curves show the raw signals that are not filtered and therefore contain some noise.

Now turning to the new approach, proposed in the dissertation, the simulation results obtained by using the flexor-extensor case depicted in Fig. 2.11(a). By using
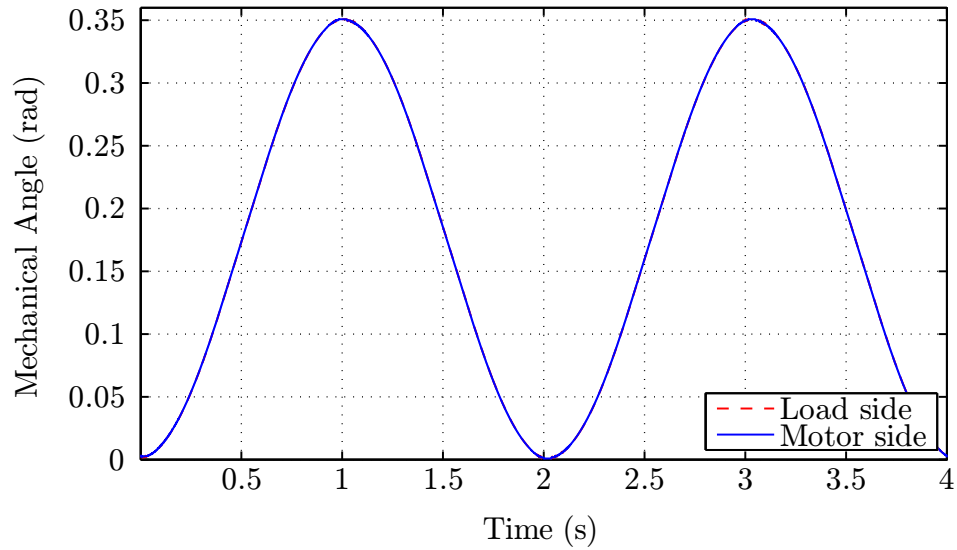
(a) Flexor-Extensor case - Simulation
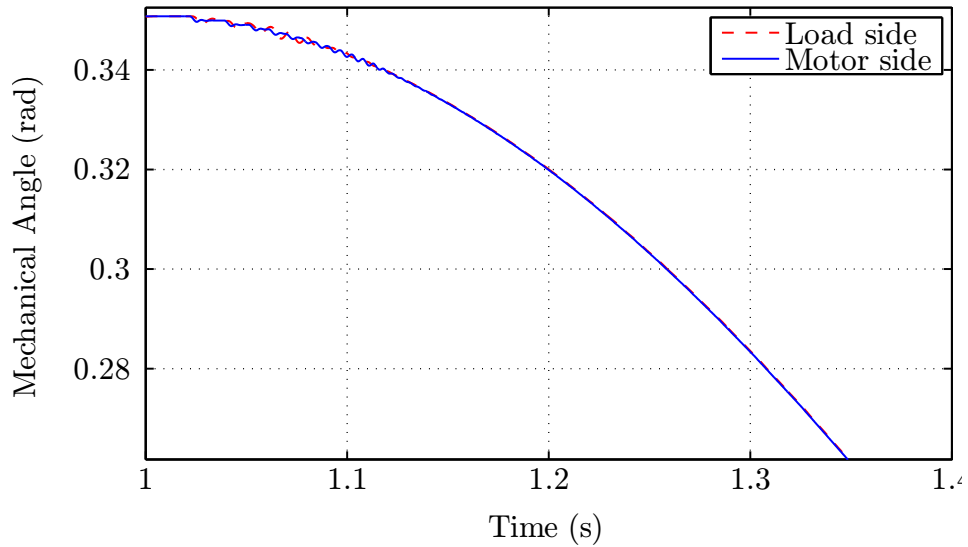
(b) Zoom at the simulation

Figure 2.11: Simulation results of the Flexor-Extensor case.

the identical reference signal that was used before and recording the same system variables, the difference between the two curves dissappear. The enlargement in Fig. 2.11(b) also shows a significant reduction.

The experimental results of this approach showes similar effect in Fig. 2.12(a). By zooming into the curves in Fig. 2.12(b) small deviations, that are comparable to the noise base of the sensor, become only noticable.
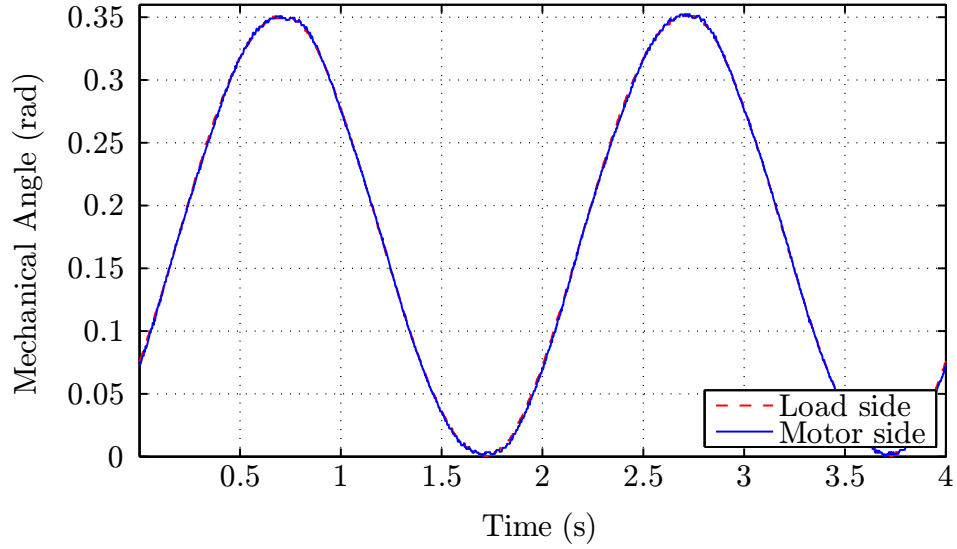
(a) Flexor-Extensor case - Experiment
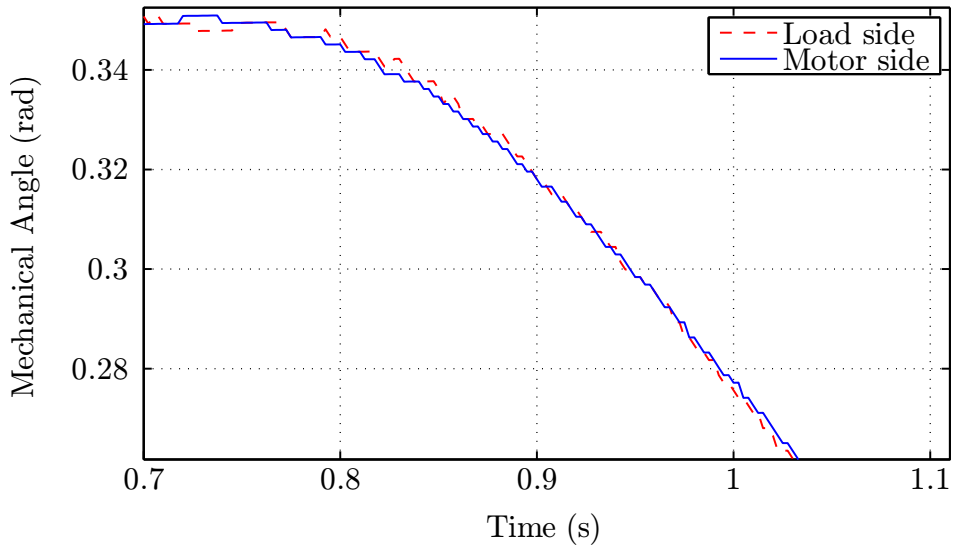
(b) Zoom at the experiment

Figure 2.12: Experimental results of the Flexor-Extensor case.

In order to have a quantitative comparison a specific mean value is defined as

$$\beta_c = \int_T \max\left(\left|\frac{\theta_l(t) - \theta_L(t)}{T}\right|, \frac{\beta_t}{T}\right) \mathrm{d}t, \qquad (2.25)$$

where T is the period of the sinusoid. This mean value gives a comparison basis to compare the results and gives an approximation of the remaining level of backlash. Table 2.1 shows the qualitative results of the four test cases. We can conclude that the standard case almost exactly reproduced the level of original backlash. In the

Table 2.1: Comparison of the results

Configuration / Method	β_c
Standard / simulation	1.913×10^{-2} rad
Standard / experiment	1.892×10^{-2} rad
Flexor-Extensor / simulation	8.7×10^{-4} rad
Flexor-Extensor / experiment	1.18×10^{-3} rad

standard case, the difference between the simulation and the experiment is about 1% (2.1×10^{-4} rad). This value for the proposed flexor-extensor case is slightly larger than 25% (-3.1×10^{-4} rad), which is caused presumably by the relatively low positional resolution, however the difference in absolute terms matches well with the preceding case. Comparing the standard and flexor-extensor case, simulation showes $1 - \frac{0.00087 \text{ rad}}{0.01913 \text{ rad}} = 95.45\%$ reduction in the avarage of the remaining backlash. Real measurement showed $1 - \frac{0.00118 \text{ rad}}{0.01892 \text{ rad}} = 93.76\%$ reduction that is just slightly less compared to the simulation result.

All constants that are used during the simulations are listed in Appendix A Table 1.

2.7 Conclusion

A new improved actuation system for robotic joints has been described in this chapter. The proposed joint consists of two stepper motors that are operated in a flexor-extensor fashion inspired by the structure of human limbs. With this solution, a method was given for minimizing the effect of backlash by applying a simple high-level control algorithm. Real measurement data show a good match with simulation results and clearly supports the practical applicability of the approach.

Based on the experimental results the mean reduction of the backlash was over 90%. More precisely, the theoretical 95.45% and the experimentally verified 93.76% results are comparable to the most effective *Switching Strategy* for backlash
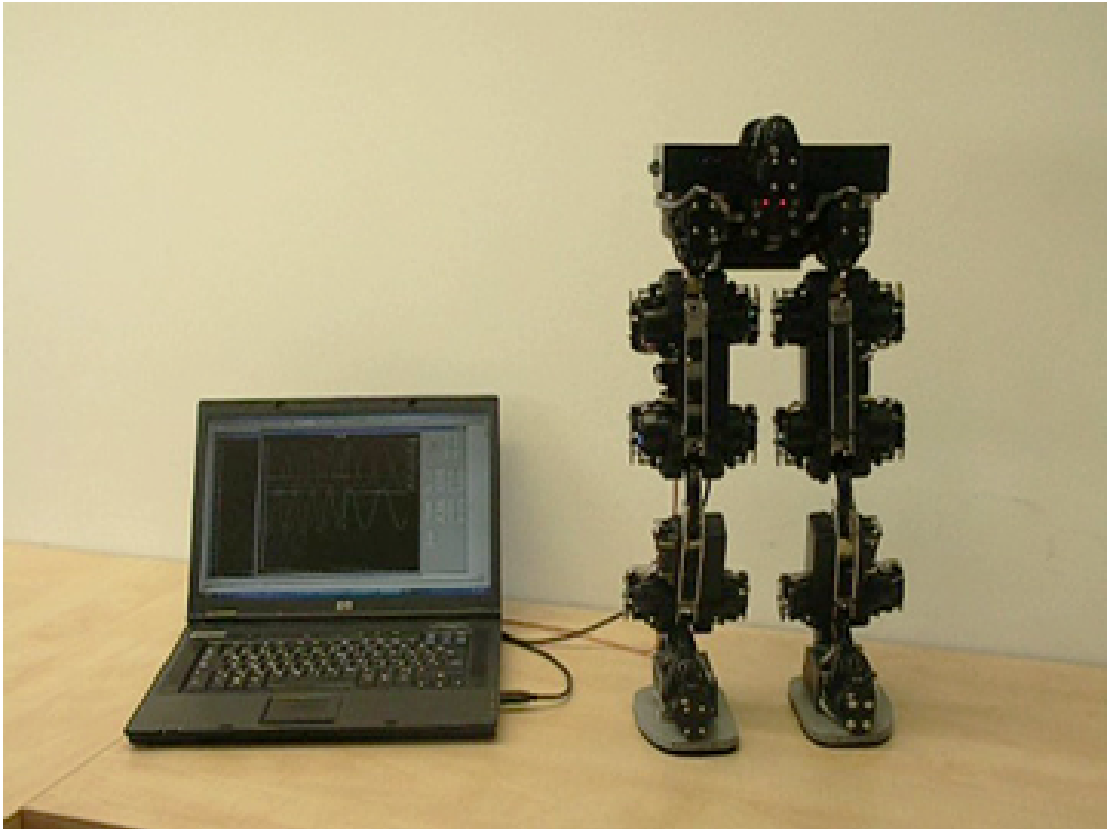
Figure 2.13: Implemented 11 DOF biped robot.

reduction that was reported [29] to reach 96.9%. However, it must be noted that the reported 96.9% is achieved with linear actuators for parallel manipulation.

In addition, our previously built biped robot [3] has been successfully enhanced by using the proposed technique to reduce the backlash of the joints. In 2009, this 11 DOF biped robot was invited to a Japanese robotic exhibition held at Tatayama, where among the state-of-the-art humanoid robots, it was presented. The robot is capable of walking in a statically stable manner. The photo of the biped robot standing next to its controlling computer can be seen in Fig. 2.13.

Chapter 3

A novel concept: The Emulated Elastic Actuator

Nomenclature

N	Pole number
θ	Angle [rad]
i	Current [A]
V	Voltage [V]
τ	Torque [Nm]
R	Resistance [Ω]
L	Inductance [H]
ω	Angular velocity [rad/s]
B	Viscous friction [N m s/rad]
J	Inertia [kg m^2]
K_T	Motor constant [Nm/A]
I	Nominal current [A]
k	Spring constant [Nm/rad]
l	Length [m]
η	Viscosity [N m s/rad]
P	Position (x,y) [m]
m	Mass [kg]
F	Force [N]
g	Gravity (9.81 m/s^2)
U	Potential energy [J]
K	Kinetic energy [J]
t	Time [s]

Superscripts

x'	Altered version of the variable x
$\dot{x}$	Newton's notation for time derivative $\dot{x} = \frac{\mathrm{d}x}{\mathrm{d}t}$

Subscripts

raw	Uncalibrated, pure encoder output
e	Electronic
m	Motor
a,b	Phase a and b
φ_a, φ_b	Binary code of phase a and b
d	Desired
$BEMF$	Back electromotive force
ref	Reference
h	Hookean
r	Resting
kv	Kelvin-Voight
s	Spring
l	free end
a	arm
cm	Center of mass
v	Virtual spring
lv	Linear Virtual spring
ns	Non-linear spring
GRF	Ground reaction force
L	Latency

3.1 Introduction

The classical robotics requires the transmission between the actuator and the load to be very stiff. This is especially true for the industrial robots where positioning accuracy is essential. Since, by increasing the stiffness precision, stability, and bandwidth of the position-control can be improved. Therefore high mechanical stiffness is combined with high feedback gain in order to achieve the desired precision in tasks like pick-and-place or robotic welding. In order to achieve positional accuracy most of the actuators use low torque electric motors with high gear ratios. The gears introduce several undesired effects like friction and backlash that can be challenging to compensate for [19]. But in the last decade the tradition of "the stiffer the better" seems to be changed.

Nowadays compliant actuator designs are gaining increasing popularity. One of the reason for that design is to overcome the limitations of a rigid transmission in terms of shock survivability, force control stability and human-safe operation. The poor shock surviving capability of the classical actuators comes from the rigidity of its structure. In addition to the lack of elasticity of the transmission the high gear ratio ($N : 1$) causes N^2 increase in reflected inertia that is why higher forces on the gears are caused by shock loads. There has been an increasing interest in the field of human-centered robotics where close interaction between robot and human become unavoidable. It was usually dangerous if traditional actuators were used since, if high reflected inertia is combined with high friction of the gearing that could easily lead to damage to the environment when unknown contact occur [39].

To address these challenges several compliant actuator designs have been published. Maybe the most interesting and the one that had the greatest impact among these is the Series Elastic Actuator (SEA) [7] that belongs to the equilibrium-controlled stiffness type. It incorporates a physical spring at the output in series with a traditional actuator. One benefit of that elasticity is that the reflected inertia of the traditional actuator part becomes hidden by the spring. It low-pass filters the shock loads but it is not without a cost, it also low-pass filters the output of the actuator. It is a trade-off that has to be accepted. Another benefit of the SEA is that the problem of force-control is turned into a problem of position-control that makes easier to exert a given force. Finally the use of a spring allows the energy to be stored that can be useful for legged locomotion to increase its efficiency. Based on this concept numerous biped robots are built.

Another group of compliant actuators is the antagonistic-controlled stiffness.

A good example for this approach is the human arm where the flexor and extensor muscles are working against each other to be able to set the position and stiffness of the arm at the same time. A simple implementation of this type was reported by Shane et al. [40]. The difficulty is that in order to be able to vary the stiffness of the antagonistic joint two non-linear springs are needed. The size of the mechanism is therefore quite big that makes it less feasible. VSA [41] and especially VSA-II [42] have a significantly smaller size but that comes for the price of a more complex structure. Another approach that falls into this category is the actuator with mechanically adjustable series compliance (AMASC) [43]. For setting the position and the compliance two separated motors are used and a biped called BiMASC was designed based on this concept.

Mechanically controlled stiffness is another type of compliant actuators where the stiffness is set by the point where an elastic element is fixed to the mechanism. A good example is MACCEPA [44] that was built with standard off-the-shelf components. This is an advantage and a disadvantage in the same time, since it is easy to build but the whole structure space requirement is not so optimal. The approach called VS-Joint [45] from the German Aerospace Center (DLR) solved this issue by creating a more compact solution.

As it can be seen numerous solutions exist to create compliant actuation. All the aforementioned designs were passive approaches that means compliance comes from the natural dynamics of the mechanism. Common advantages of this kind of compliant actuators are the simple control, inherent safety and good efficiency. The drawbacks are their more complicated mechanism, their bigger size, weight and usually these require two sperate motors that increase the cost. Though, there are simpler designs like the SEA that can be more optimal but these are having a pre-selected stiffness and it can only be changed by manually replacing the elastic element to a proper one.

Besides passive compliance, there is active compliance where compliant behaviour is achieved by changing actively the natural dynamics of the mechanism. A good example is the Lightweight Robot series (LWR I, II, III) [46] created by the DLR. It belongs to the soft-robotics and features joint level torque control. The idea is to have a harmonic drive with high-gear ratio that already have some compliance. Then incorporating a torque sensor and a position sensor the compliant behaviour is reached with the help of a high-level control. Since the actuator is hardly backdrivable it is crucial to have a fast feedback loop otherwise performance and safety would degrade. That is why, a high 3 kHz update rate is used

3. A NOVEL CONCEPT: THE EMULATED ELASTIC ACTUATOR

even though during a sudden change in contact forces can easily exceed that limit.

Another way of creating active compliant actuation is by using SEA with active control. Radkhah et al. [47] presented a feedforward controlled emulated spring stiffness based approach. An SEA is used which have a fixed mechanical stiffness but setting the zero-torque position of the spring dynamically a "virtual stiffness" is achieved. The advantage of this design is its simplicity since it does not require any torque sensor or complex computation. The drawback is the lack of feedback that creates deviation from the expected result.

Bigge et al. [48] created a similar design with feedback. The elastic element is used as a torque sensor by measuring the angle of deflection. PID control is used to track the desired force profile that has been set according to the desired virtual spring characteristic. The benefit of the solution is that it can utilize the advantages of the original SEA like the improved shock survivability or the more stable force control. The drawback is the limited output response rate due to the incorporating SEA.

In the light of the foregoing, I propose a new concept of fully electric emulation of joint elasticity for biped robots and for other applications (patent pending). I call it Emulated Elastic Actuator (EEA) after the SEA since, in fact it is an actuator that features emulated elastic behavior. The idea is to come up with a mechanism that has very low gear ratio, that is highly backdrivable, and has practically zero backlash and then use an electric motor, under a proper control, to produce the required torque in every time instance to mimic the behaviour of a physical spring. The first criterion, namely the low gear ratio, is necessary to handle the aformentioned problem of reflected inertia. The second one is closely related, since high gear ratio usually means high level of friction that when combined with high inertia yields to low backdrivability. The third one, the hard non-linearity of the transmission, has already highlighted in Chapter 2. It can be observed that, in almost all robotic applications these three criteria are not met at the same time. Even, by using the industrial standard harmonic drive, to have the transmission free of backlash, the joints become hardly backdrivable due to significant level of friction. The reason why high gear ratios are used lies in the type of electric motors that are used by the engineering community.

Nowadays, in the field of robotics brushed Direct Current (DC) motors are getting replaced by Brushless DC (BLDC) motors. The successor less prone to wear out and features significantly less electromagnetic interference (EMI). Nevertheless, the operating speed of these motors has not been changed. These are usually

designed for thousands of RPM, which is far beyond the speed where the robotic joints are operated. Obviously, these motors need gears with high gear ratios, otherwise the actuators would be operated in a much lower efficiency region. A solution would be using motors with significantly lower speed but those are not commercially available.

Off-the-shelf stepper motors are designed for lower speed, but are used in a substantially different operating scheme. As the name implies stepping is the desired motion of these motors. By properly energizing the coils of a stepper motor discrete steps are done, contrast to the DC motos where constant coil current creates continuous motion. Based on these, it is very unusal to use stepping motors in robotic joints, however those motors are mass produced and are designed for lower speed. To prove the advantages of the stepping motors over the ones that are currently used Fig. 3.1 shows a comparison of few different commercially available electric motors. The EC family is the product of the Maxon Motor Inc., 3268 024 BX4 is produced by FAULHABER Inc., DBE-2000-H-1ES belongs to Moog Inc., and the remainder are the hybrid stepper motors fabricated by the Linengineering Inc. It is a common approach to compare different motors by the motor constant. However, the selected motors are about the same weight but are
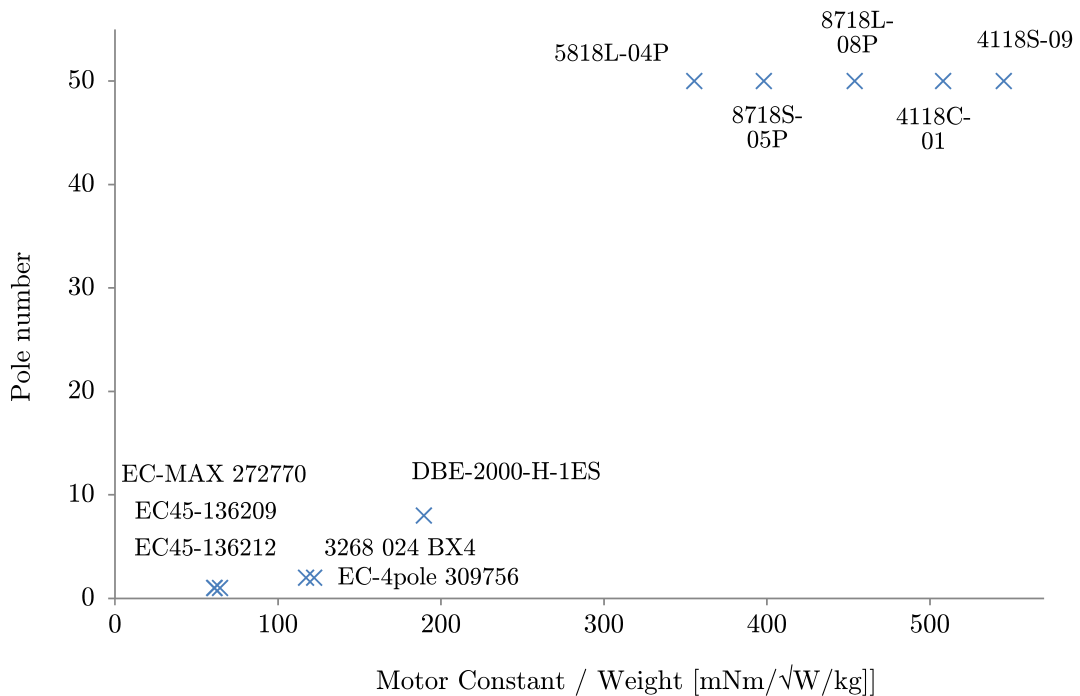
Figure 3.1: Comparison of different off-the-shelf electric motors.

normalized to unit mass to improve the comparison. Surprisingly, all the motors with high motor constant belongs to the stepper type. The reason for that is the significantly greater number of poles that we can found in the stepper motors. This is in accordance with our previous statement since lower the pole number higher the speed.

We can conclude that, contrary to engineering practice, using stepper motor in a robotic joint can help us to meet the aformentioned criteria. But in the same time in order to use this type it requires a considerably different scheme of operation. In Section 3.3, the detailed model of the hybrid stepper motor (HSM) will be presented.

3.2   Concept of the Emulated Elastic Actuator

First of all, let's consider a situation where gearing is neglected and therfore direct drive is assumed. As already pointed out in the previous section, HSM is a promising alternative for the industry standard BLDC. Afterwards, equip the motor with a position sensor. It is preferred to be a magnetic encoder, but not limited to that type, optical or capacitive encoders could be used. The advantage of the magnetic type is that it is less prone to malfunction caused by dust (in Section 3.6, further comparison is carried out). In addition to the encoder, place a motor driver and a local controller that has moderate computational capability. Fig. 3.2 shows a possible arrangment of the system parts. The motor driver is preferred to be a transconductance type to achieve an accurate current control. In contrast to the industrial standard HSM commutation scheme, precise torque control must be used, that will be covered in Section 3.3. Now, we have a system that is capable of sensing its position and roughly speaking can be used to produce an arbitrary torque.

Based on these, in the following I am going to investigate the possibility of shaping the natural dynamics of the system by high-speed local control. More precisely, to design and implement an actuator that is capable of emulating different
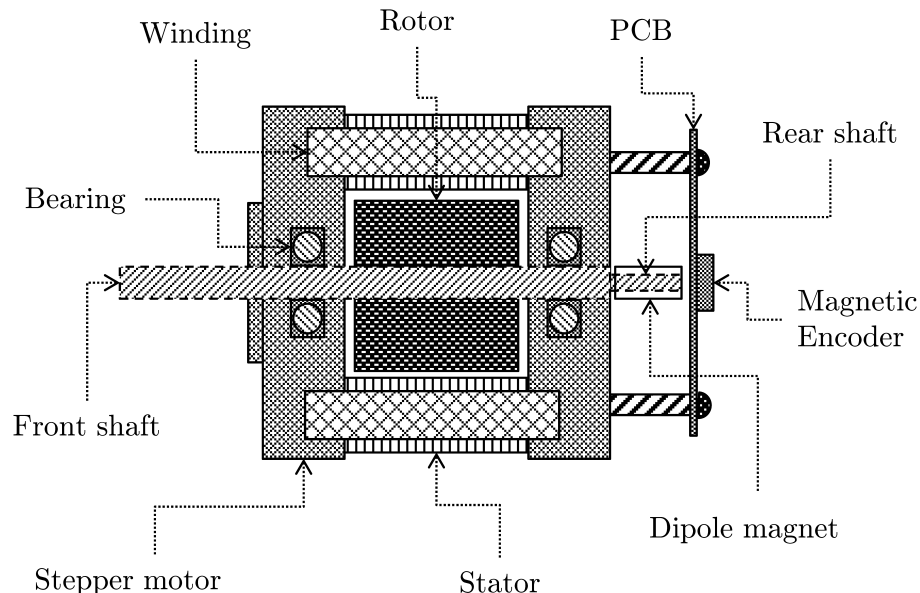
Figure 3.2: A hybrid stepper motor with local controller.

3. A NOVEL CONCEPT: THE EMULATED ELASTIC ACTUATOR

types of elastic behavior. In other words, to come up with a new concept of a universal actuator that can be used to change the way how it interacts with its environment.

The most important requirement is that the control must be local, in order to be able to realize high-speed operation (more than 20.000 iteration/sec). Until recently, the typical fastest torque control was in the range of 1-2 thousands of iteration per second, which is slower at least of one order than the proposed one. A slower global control could be used to alter the parameters of the desired elastic behavior.

Importantly, high speed operation must be supported at commutation level. Fig. 3.3 illustrates the block diagram of the proposed low-level system. The raw output of the encoder (θ_{raw}) is used for the calculation of the motor's actual position (θ_m) and the "electronic" angle (θ_e) that is necessary for the torque linearization. In Section 3.3 the details of the motor characteristic's linearization will be given. The result of the linearization is two instantenous coil currents (i_A and i_B) therefore a precise current control circuit is needed. For that purpose a Pulse-Width Modulation type motor driver is used that requires voltage as input to control
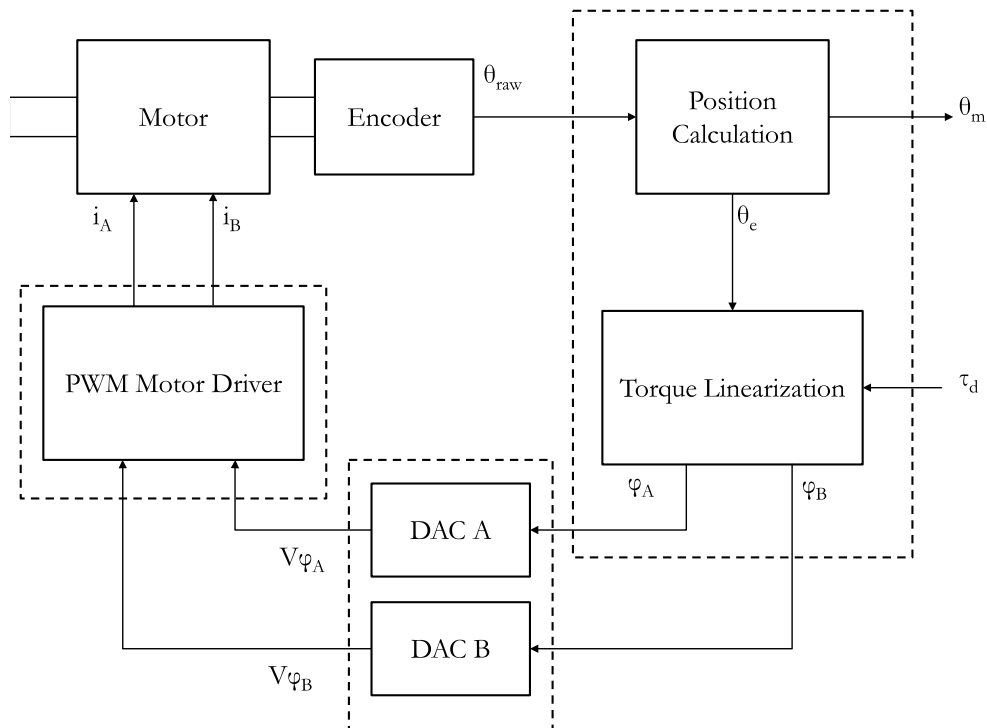
Figure 3.3: Block diagram of the electronic commutation.

the current. V_{φ_A} and V_{φ_B} are the two input voltages that are the outputs of the two Digital-to-Analog Converters (DAC A and DAC B). The binary codes of the voltages are φ_A and φ_B.

The calculation of the position and the linearization of the motor's characteristic is executed at the same 32-bit microcontroller (PIC32MX340F512H from Microchip Inc.) which iterates the emulation. The encoder is a TLE5012 from Infineon Inc., and the motor driver is a TMC246A (Trinamic Inc.). The complete electrical schematic is given in the Appendix.

The input of this subsystem is the desired motor torque (τ_d) and the output is the current angular position of the motor (θ_m). The idea is to create a fast feedback loop, that is iterated at 22 kHz, between θ_m and τ_d in order to be able to emulate different kind of elastic behaviors.

In order to further investigate the concept, the detailed model of the HSM will be presented.

3.3 Model of the hybrid stepper motor

Hybrid stepper motors are combining the principles of variable-reluctance and the permanent magnet stepper motors, that was used in the previous chapter. The detailed investigation of the motor, however, is beyond the scope of the dissertation thus, only the details that are strongly related to the subject will be covered. Therefore, the two phases (A and B) of a hybrid stepper motor having the following instantaneous torques

$$\tau_A = -K_T i_A \sin(\theta_e) \tag{3.1}$$

$$\tau_B = K_T i_B \cos(\theta_e), \tag{3.2}$$

where higher harmonics are neglected, K_T is the motor constant, i_A and i_B are the coil current in phase A and B, respectively and

$$\theta_e = \theta_m N \tag{3.3}$$

is the "electronic" or commutation angle, where θ_m is the position of the motor's shaft and N is the number of poles.

In fact, due to fabrication inaccuracies the real torques (Fig. 3.4) differ from our approximation, but it is a common approach to assume (3.1)-(3.2).

The total torque produced by the motor can be written as the sum of the two
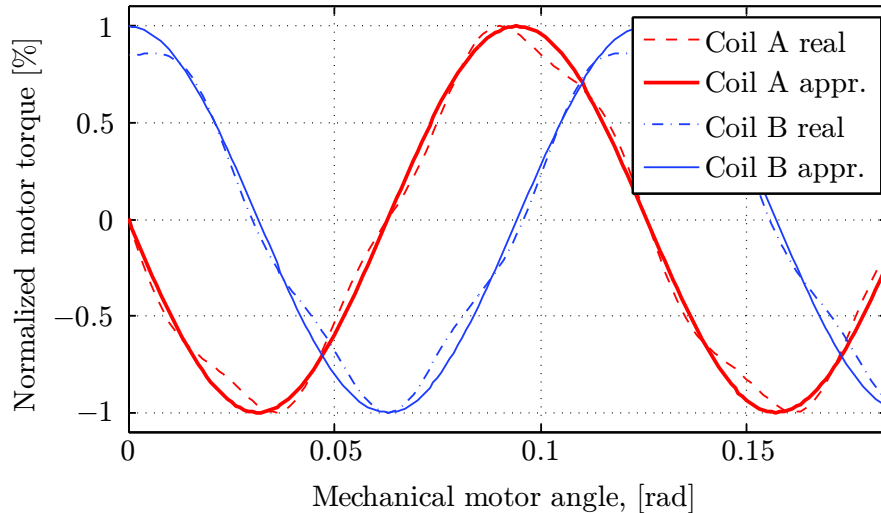
Figure 3.4: This figure shows the instantaneous torque produced by the two phases being energized at the rated current.

3. A NOVEL CONCEPT: THE EMULATED ELASTIC ACTUATOR
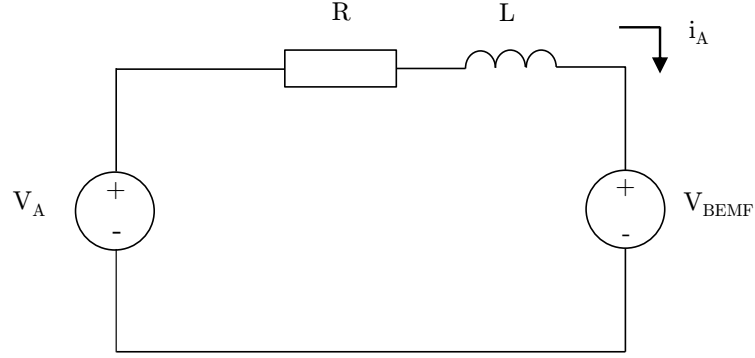
Figure 3.5: Equivalent circuit of phase A of the stepper motor.

phases due to their independent nature

$$\tau_m = \tau_A + \tau_B. \tag{3.4}$$

The electric model of the motor is a closed circuit with an ohmic part, an inductive part and a voltage source. Fig. 3.5 shows only the equivalent circuit of phase A for brevity, where the two phases are considered to be independent. According to this, the rate of change of the current flowing through the coil A and B are formulated in the following way

$$\frac{\mathrm{d}i_A}{\mathrm{d}t} = \frac{v_A - Ri_A + K_T\omega\sin(\theta_e)}{L} \tag{3.5}$$

$$\frac{\mathrm{d}i_B}{\mathrm{d}t} = \frac{v_B - Ri_B - K_T\omega\cos(\theta_e)}{L}, \tag{3.6}$$

where the voltage source symbolizing the counter-electromotive force was subtitued with

$$V_{BEMF} = K_T\omega\sin(\theta_e). \tag{3.7}$$

Now turning to the mechanical model of the motor, with only viscous friction involved, it can be written in the following way

$$\frac{\mathrm{d}\omega}{\mathrm{d}t} = \frac{\tau_m - B\omega}{J} \tag{3.8}$$

$$\frac{\mathrm{d}\theta_m}{\mathrm{d}t} = \omega, \tag{3.9}$$

where B ($\mathrm{N\,m\,s/rad}$) is the viscous friction coefficient and J ($\mathrm{Kg\,m^2}$) is the inertia of the rotor. We can conclude that, a constant voltage on phase A or B will not

3. A NOVEL CONCEPT: THE EMULATED ELASTIC ACTUATOR

produce the desired continous motion, but will do a discrete step. Obviously, that is why these motors are used for application like fine-positioning, etc.

In order to use these motors for our purposes the non-linear relation of the motor torque on the input current, needs to be linearized. Bodson et al.[49] reported the stepper motors to be feedback linearizable. By a proper choice of input currents it can be transformed into a new linear form. Let's assume that the coil currents are chosen to be in the following way

$$i_{Aref} = -I_{ref}\sin(\theta_e) \tag{3.10}$$

$$i_{Bref} = I_{ref}\cos(\theta_e), \tag{3.11}$$

then by substituting (3.10) and (3.11) into (3.4) the torque of the motor becomes

$$\tau_m = K_T I_{ref}\sin^2(\theta_e) + K_T I_{ref}\cos^2(\theta_e) = K_T I_{ref}, \tag{3.12}$$

where trigonometric identity was used. It can be easily seen that the new expression shows linear relationship between the motor torque and I_{ref} which means direct torque control of the stepper motor is possible by measuring the shaft position and using it as a feedback.

Please note that, current saturation and other limitations are neglected for this time, but in Section 3.6 these are thoroughly analyzed.

To be able to accuratly model the motor, the dynamics of the driver cannot be ommited. The emulation needs precise current control and therefore standard constant voltage type driver would be inappropriate. Thus, transconductance type is used (TMC246A from Trinamic Inc.). The accurate operation of the integrated circuit is not public (patent pending), as a result an approximated model will be used instead. There are two independent current loops that try to maintain the desired level of coil current. Pulse Width Modulation (PWM) is used to build up or decay current. Let's modify V_A and V_B in (3.5) and (3.6) to include the inner dynamics of the driver

$$V_A'(i_A) = \begin{cases} -V_{max} & i_A > i_{Aref} \text{ and } i_{Aref} < 0 \\ V_{max} & i_A < i_{Aref} \text{ and } i_{Aref} > 0 \\ \frac{-V_{max}}{3} & i_A > i_{Aref} \text{ and } i_{Aref} > 0 \\ \frac{V_{max}}{3} & i_A < i_{Aref} \text{ and } i_{Aref} < 0, \end{cases} \tag{3.13}$$

3. A NOVEL CONCEPT: THE EMULATED ELASTIC ACTUATOR
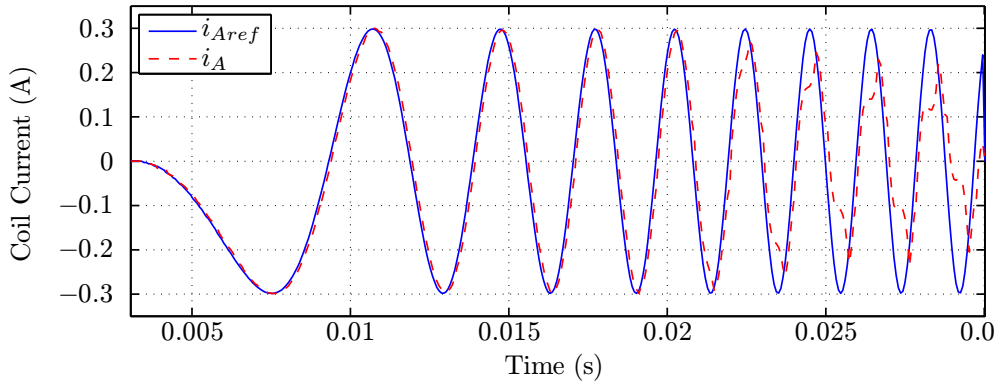
(a) Simulation result
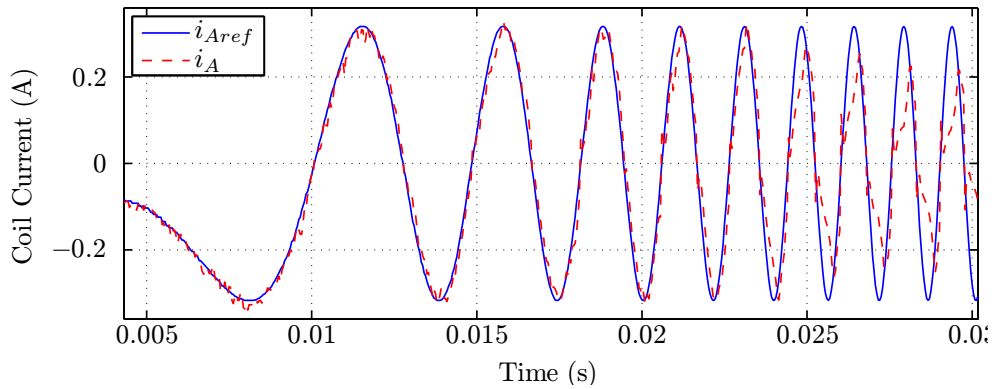
(b) Experimental recording

Figure 3.6: Free acceleration due to constant torque (i_A versus i_{Aref}).

where V_{max} is the available supply voltage and $V'_B(i_B)$ takes a similar form, hence ommited for brevity. Actual numbers were manually tuned to capture the real dynamics at an acceptable level. In order to verify the effectiveness of the approximation Fig. 3.6 shows a comparison of the simulation and experimental data for the same input. From resting, the motor was commanded to constantly accelerate with the quarter of the rated current. According to (3.10) current reference were sinusoidal. The reference (i_{Aref}) and the actual (i_A) currents are plotted for phase A. As the motor accelerated, due to the constant torque, the frequency of the sine shape increased. At a certain point, the real signal started to lag behind the reference, that was accurately captured by the simulation. In Section 3.6, the accurate phenomenon is discussed in more detail.

In the rest of the chapter this modified motor model will be used.

51

3.4 Linear type elasticity: Hooke and Kelvin-Voight model

First of all, let's consider the simplest elastic behavior, the Hookean. For rotational motion, in case of a torsional spring, Hooke's law states the following

$$\tau_h = -k_h \Delta\theta_h, \tag{3.14}$$

where τ_h is the restoring torque exerted by the spring, k_h is the spring constant (Nm/rad) and $\Delta\theta_h$ denotes the angle of deflection from the resting point of the spring. The minus sign implies that the exerted torque is opposite in direction of the deflection. It is a common approach in engineering applications to model many materials, for example the steel, with this linear equation.

Based on these, one can formulate the dynamics of a torsional spring that is fixed at its one end and freely moving at the other end

$$\frac{\mathrm{d}^2\theta_s}{\mathrm{d}t^2} = \frac{-k(\theta_r - \theta_s)}{J_l}, \tag{3.15}$$

where θ_s is the angular position of the free moving end of the spring, θ_r is the resting angle and J_l is the inertia of the free moving end.

In order to emulate a Hookean linear elastic behavior with our actuator, the following layout is considered. The motor is considered to be attached to a table by setting the motor shaft perpendicular to the plane of the table. Fig. 3.7 illustrates the arrangement, where an l long arm with negligeble mass connects the shaft with
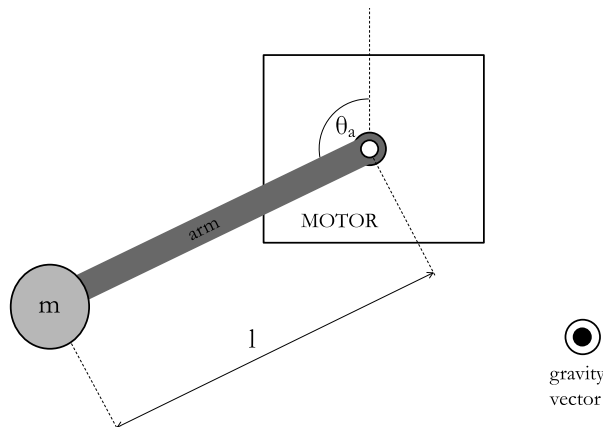
Figure 3.7: Schematic of the layout for the linear elastic behavior's emulation.

3. A NOVEL CONCEPT: THE EMULATED ELASTIC ACTUATOR

the m point mass, and the angle of the arm is denoted by θ_a. Now let's write the equation of motion for this configuration

$$\frac{\mathrm{d}^2\theta_a}{\mathrm{d}t^2} = \frac{\tau_m}{J_a}, \tag{3.16}$$

where τ_m is the torque of the motor, $J_a = l^2 m$ is the total inertia of the arm and friction is neglected. Please note that, the contribution of the gravity is zero, the reason for that is the plane where the motion is perpendicular to the gravity vector.

In the light of (3.12) we can come up with an I_{ref} to realize the required $\tau_m = -k(\theta_r - \theta_a)$ that would emulate the elastic behavior

$$I_{ref} = \frac{-k(\theta_r - \theta_a)}{K_T}. \tag{3.17}$$

Now, if we substitute (3.17) into (3.12) and numerically simulate (3.16) it must end up with an undamped oscillatory motion, that can be followed in Fig. 3.8.
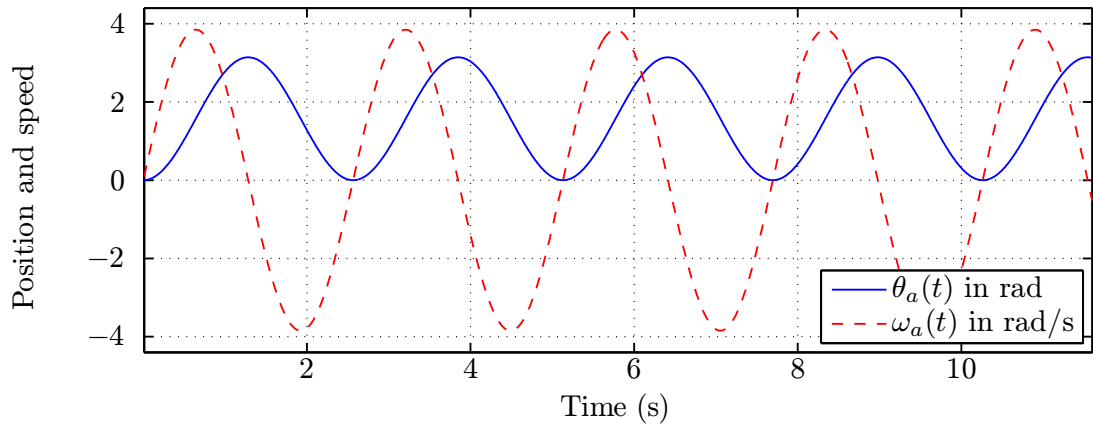
Figure 3.8: Simulation of the Hooke type elastic behavior

The initial condition of the differential equation was set to $\theta_a(0) = 90°$ and $\omega_a(0) = 0$. The inertia was $J_a = 6.5 \times 10^{-3}$ Kg m^2 and the spring constant was set to $k = 44.5$ Nm/rad.

Experimental data with the same initial conditions were conducted (Fig 3.9). It can observed that, in contrast to the simulation the oscillation tends to decay. The reason for that is the false assumption of no viscous friction is involved. In fact, there is no physical system without energy dissipation. In order to emulate Hookean elastic behavior the energy dissipation must be compensated.

Once the required compensation is achieved, the system started to oscillate

3. A NOVEL CONCEPT: THE EMULATED ELASTIC ACTUATOR
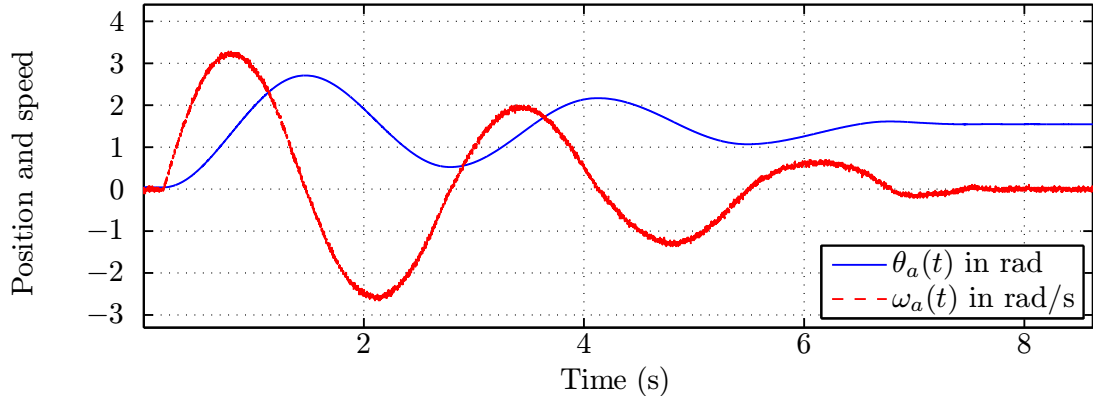
Figure 3.9: Experimental result of the Hooke type elastic behavior

with a negligible level of damping. Fig. 3.10 demonstrates the previous statement, since it shows the same behavior as we seen in Fig. 3.8.
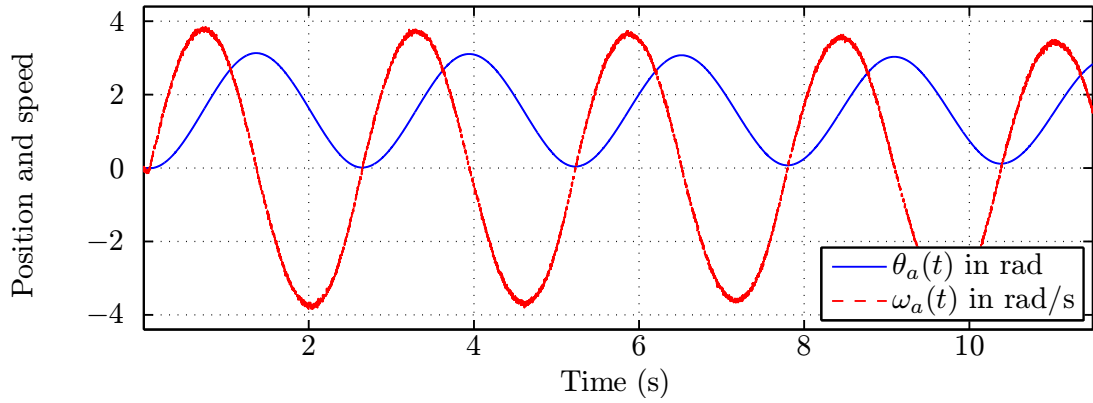
Figure 3.10: Experimental result of the Hooke type elastic behavior with compensation

In terms of energy dissipation, in contrast to Hookean model, which conserves the energy, Kelvin-Voight model is told to be dissipative. This is another simple linear model to describe a different elastic behavior. It consists of a linear spring and a speed dependent damper connected in parallel. One can formulate the governing equation for rotational motion as follows

$$\tau_{kv} = -k\Delta\theta_s - \eta\frac{\mathrm{d}\theta_s}{\mathrm{d}t}, \tag{3.18}$$

where τ_{kv} is the exerted torque due to spring and the damper, and the η is the viscosity (N m s / rad). The second term responsible for the damping, since it acts always in the opposite direction of the motion. Similarly as in the case of the

3.   A NOVEL CONCEPT: THE EMULATED ELASTIC ACTUATOR

Hookean (3.17) we can come up with an I_{ref} to realize this kind of elastic behavior.

Now let's consider the same initial conditions and spring constant that was used to simulate Fig. 3.8, but add a viscous damping to the emulation according to (3.18). Let the value of the viscousity be $\eta = 1.5 \times 10^{-3}$ N m s / rad. The effect of the damping can be followed in Fig. 3.11(a). It can be observed that, the behavior mimics an overdamped spring-mass system.

In order to have a side-by-side comparison, Fig. 3.11(b) shows the experimental data of the emulation. The result shows good match with the previous numerical simulation. Due to the low speed of the motion, the noise of the angular speed signal become visible.
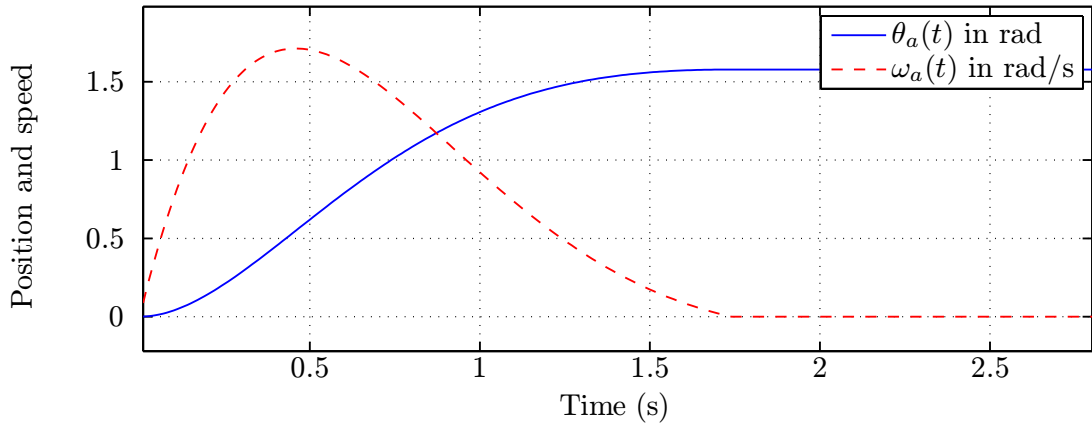
(a) Simulation result
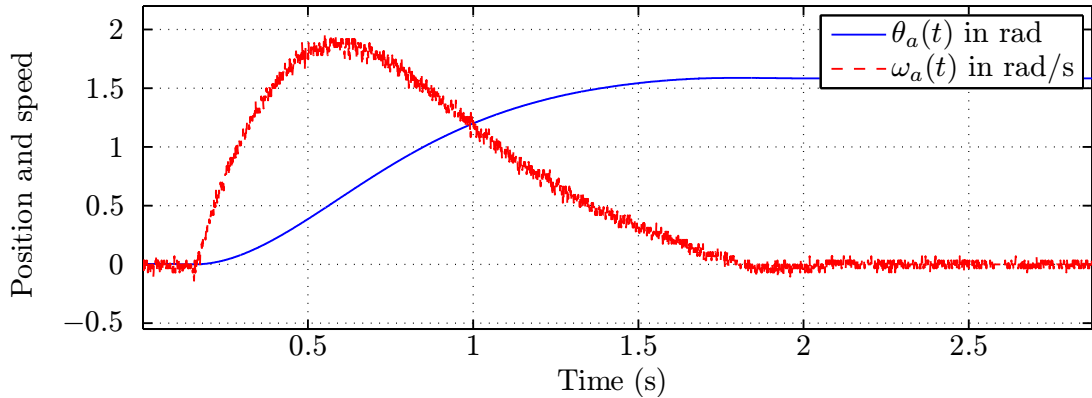
(b) Experimental recording

Figure 3.11: Kelvin-Voight type of elastic behavior with high level of viscousity ($\eta = 1.5 \times 10^{-3}$ N m s / rad).

3.4.1 Positive damping

Obviously, arbitrary model parameters could be used, as long as the limitations (Section 3.6) are taken into account, but a few more results will be given with different parameters. First, let's increase now the stiffness of the spring to four times of its previous value and choose a viscousity that is equal to the viscous friction of the actuator ($\eta = B$). Other system parameters remain unchanged.

For a given inertia, the higher the stiffness, the higher the frequency of the oscillation. This is in agreement with the numerical simulation that is depicted in Fig 3.12(a).

In terms of the experimental results, slight variation could be caused by the fact that the experiments were started manually, that affects the initial conditions. However, despite the previosly mentioned drawback the same damped harmonic oscillation was measured. The corresponding result is depicted in Fig. 3.12(b).
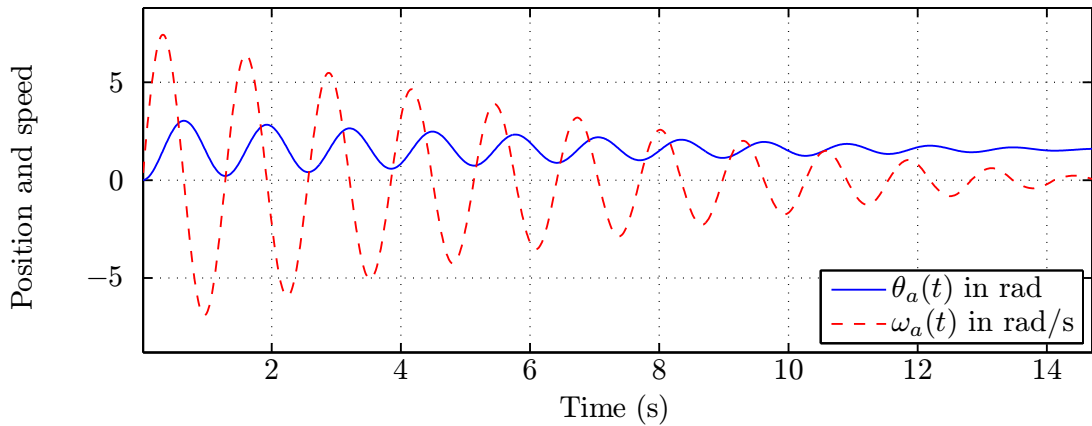
(a) Simulation result
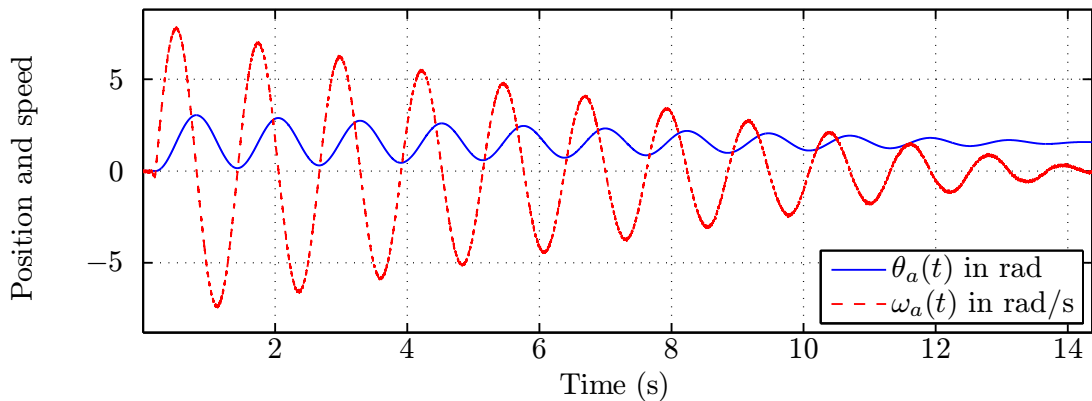
(b) Experimental recording

Figure 3.12: Damped harmonic oscillation with $k = 178$ Nm/rad and $\eta = B$.

3.4.2   Negative damping

Until recently, only passive systems were emulated. However, the proposed concept is not limited to that type, but capable of realizing active one as well.

Let's consider a negative η. In that case the damping turns to be negative. It can be easily seen that, over time, the oscillation will increase in magnitude. Since, the rise is not limited the system is unstable. One practical use of the negative damping is to be able to compensate for the viscous friction of the actuator.

Fig. 3.18(a) shows the result of the simulation with $\eta = -1.28 \times 10^{-3} \, \mathrm{N\,m\,s}$ / rad. And finally Fig. 3.18(b) shows the experimental data that is in agreement with the simulation.

(a) Simulation result

(b) Experimental recording
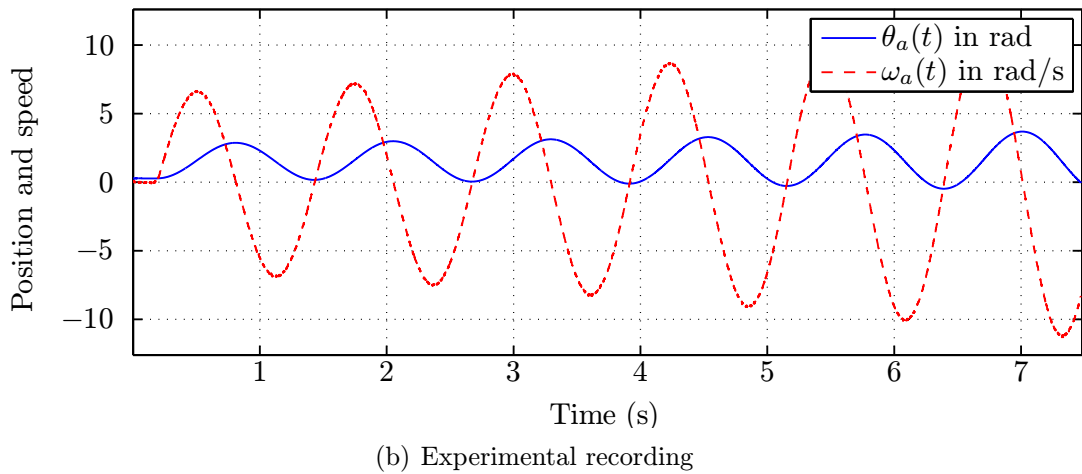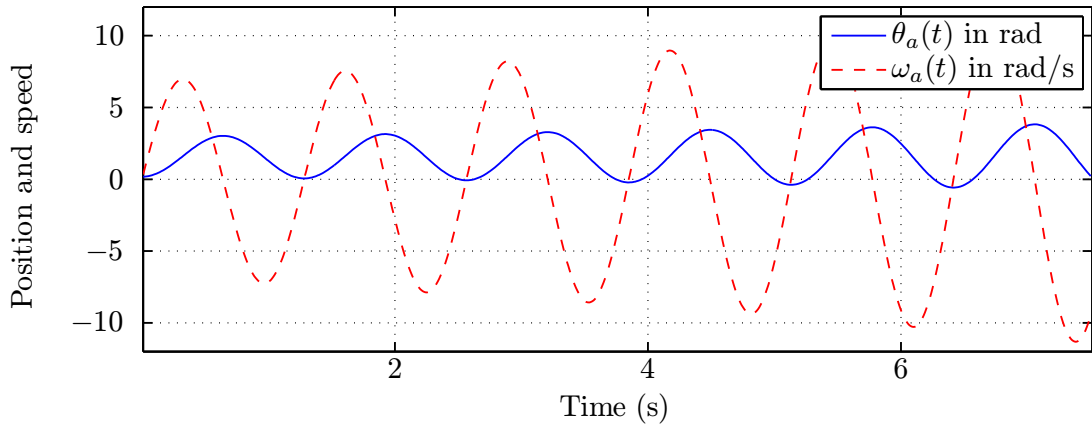
Figure 3.13: Example for negative damping ($\eta = -1.28 \times 10^{-3} \, \mathrm{N\,m\,s}$ / rad).

3.5 Non-linear type elastic behavior for legged robots

In the previous section, emulation of linear torsional spring was investigated. Apparently, the concept of the EEA is not limited to linear elastic behavior. In the following, the proposed concept of software emulation of elasticity will be extended to non-linear case.

It is a common approach to model our legs as springs [50, 51]. During touch-down, the compression of the virtual spring imitates the behavior of the leg as it is trying to absorb the impact. Fig. 3.14 demonstrates the touch-down phase of a human walking or running.

Apparently, not only the human legs can be modeled as springs but the biped robots as well. Iida et al. [52, 53] have demonstrated how linear springs can improve walking and running capability of human-like biped robots. Nevertheless, in order to relalize even a simple linear virtual spring, non-linear elastic behavior is required at the joints. Therefore, it is not enough to have linear torsional springs at the joints but spring with non-linear function must be used.

In this section, this question will be investigated with the help of an underactuated, one legged robot.
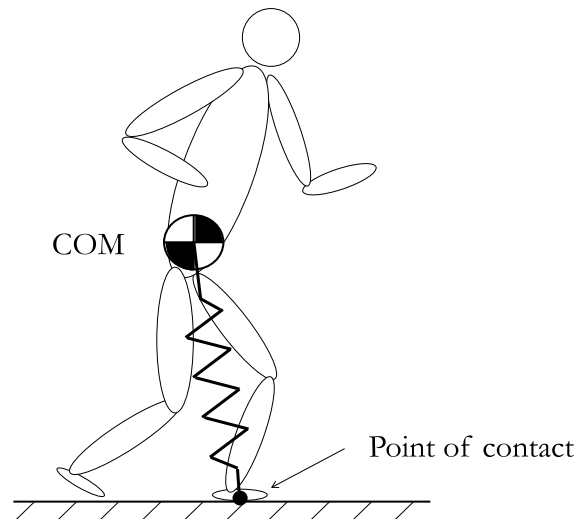
Figure 3.14: Leg modeled as linear spring attached between the center of mass of the body and the contacting point on the ground.

3.5.1 Underactuated, one legged robot with two degree-of-freedom

Let's consider the simplest legged robot, a mechanism with only one leg. More precisely the one dimensional version of that where the robot is constrained to move along the vertical axis. Fig. 3.15 illustrates the 2D kinematic description of the system. For its two degree-of-freedom(DOF), one is the angle (θ) measured between the lower ("shank") and upper ("tibia") link. The other one is the distance (y_0)
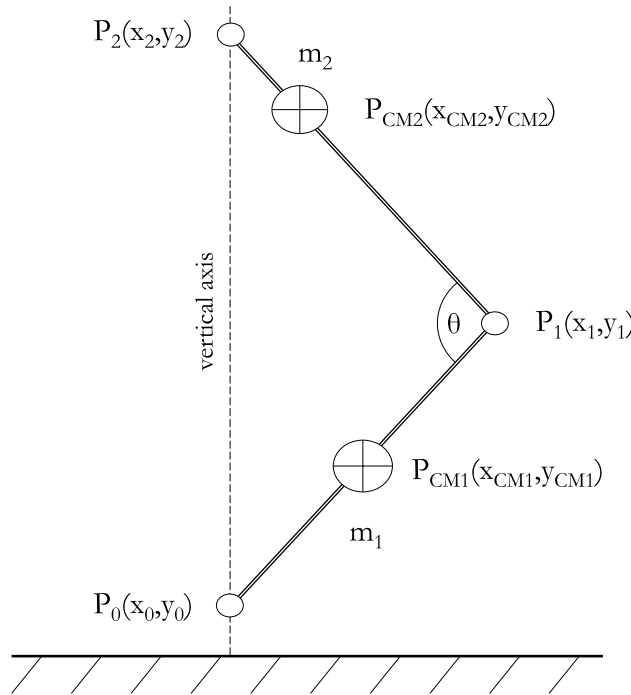
Figure 3.15: 2D kinematic description of the proposed one legged robot.

between the robot's "foot" (P_0) and the ground (0,0). In contrast to classical robotics, where manipulators are always attached to the ground and fully actuated, this is underactuated. It means, there is no direct control over the second DOF.

As already pointed out, the robot's "foot" (P_0) and its "hip" (P_2) are constrained to the vertical axis, therefore $x_0 = x_2 = 0$. The length of the links (l) are symmetric, but the weights of the links (m_1,m_2) and the relative position of the COMs are asymmetric.

Now, the task is to implement a linear virtual spring between the point of the COM of the body and the contact point on the ground. To start with, assume $m_1 << m_2$ and P_{CM2} is very close to P_2, therefore the spring should act between P_0 and P_2 along the vertical axis.

3. A NOVEL CONCEPT: THE EMULATED ELASTIC ACTUATOR

First of all, let's consider the resulting force-distance characteristic of the virtual spring in the case when linear torsional spring is used at the "knee" joint (P_1). Assume a simple Hookean elasticity with spring constant of k_s

$$\tau_s = -k_s(\theta_r - \theta), \tag{3.19}$$

where θ_r is the resting angle. Now, the force exerted by the virtual translational spring can be defined as

$$F_v(\theta) = \frac{\tau_s}{l\cos(\frac{\theta}{2})}. \tag{3.20}$$

To get the force-distance characteristic of the virtual spring (3.20) can be rewritten to be function of y_2

$$F_v(y_2) = \frac{-k_s[\theta_r - 2\arcsin(\frac{y_2}{2l})]}{l\cos[\arcsin(\frac{y_2}{2l})]} = -k_s\frac{\theta_r - 2\arcsin(\frac{y_2}{2l})}{l\sqrt{1 - \frac{y_2^2}{4l^2}}}, \tag{3.21}$$

where $y_2 = 2l\sin(\frac{\theta}{2})$ and trigonometric identity was used. It is easy to see that, (3.21) shows a non-linear force-distance characteristic. For a given length $(l = 1\,\text{m})$, torsional spring constant $(k_s = 1\,\text{Nm/rad})$ and resting angle $(\theta_r = 55°)$ the plot of the virtual spring characteristic is depicted in Fig. 3.16.

Therefore, in order to end up with a linear virtual spring characteristic, a non-linear joint elasticity must be realized. Let's define the new non-linear torsional
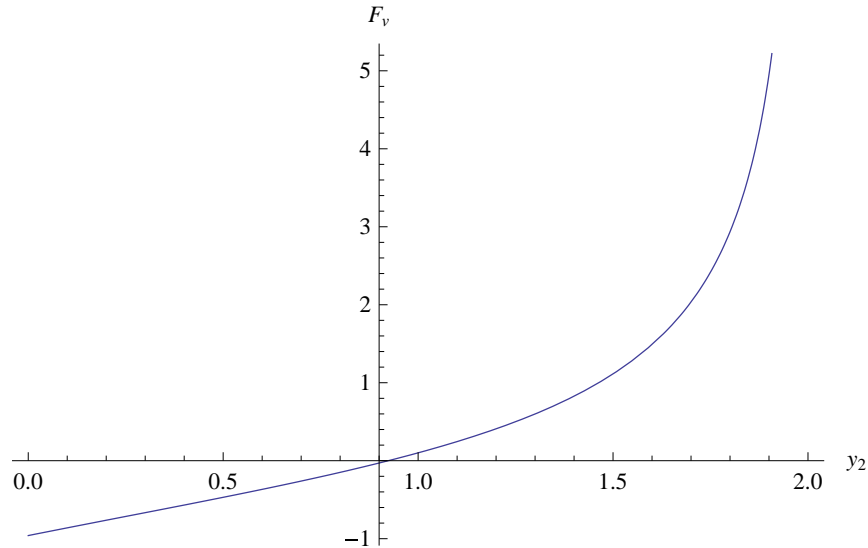
Figure 3.16: Non-linear force-distance characteristic $F_v(y_2)$ of the resulting virtual spring in case of the linear torsional elasticity.

3.   A NOVEL CONCEPT: THE EMULATED ELASTIC ACTUATOR

elasticity in the following way

$$\tau_{ns} = -2k_{ns}l^2 \cos\left(\frac{\theta}{2}\right)\left[\sin\left(\frac{\theta_r}{2}\right) - sin\left(\frac{\theta}{2}\right)\right], \tag{3.22}$$

where the index $_{ns}$ denotes the non-linear spring. The $\tau_{ns}(\theta)$ is the torque-deflection characteristic of the new torsional elasticity. For given parameters $(k_{ns} = 1, l = 1, \theta_r = 45°)$ this new charactaristic is plotted in Fig. 3.17.
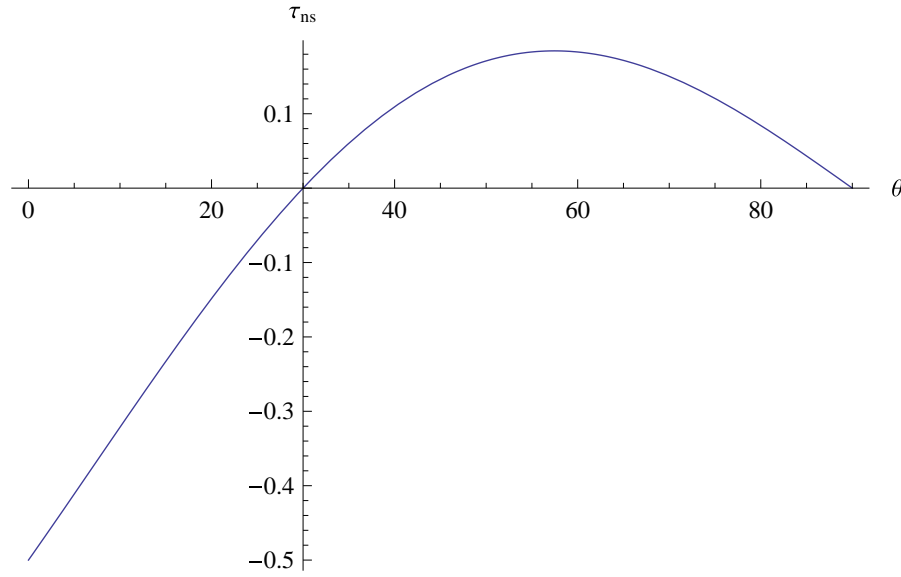
Figure 3.17: Non-linear torque-deflection characteristic $\tau_{ns}(\theta)$ of the joint elasticity intended to realize the desired linear virtual spring.

It is easy to see that, now (3.21) fullfills the linearity regarding of the virtual spring betweeen the "foot" and the "hip". It can be verifyed by substituting (3.22) to (3.20) as we did before

$$F_{lv}(\theta) = \frac{-2k_{ns}l^2 \cos\left(\frac{\theta}{2}\right)\left[\sin\left(\frac{\theta_r}{2}\right) - \sin\left(\frac{\theta}{2}\right)\right]}{l \cos\left(\frac{\theta}{2}\right)} = -2k_{ns}l\left(\sin\frac{\theta_r}{2} - \sin\frac{\theta}{2}\right), \tag{3.23}$$

that can be rewritten to be function of y_2, similarly like in (3.21), we end up with the desired linear virtual spring

$$F_{lv}(y_2) = -k_{ns}(y_r - y). \tag{3.24}$$

It can be concluded that, non-linear elastic behavior like in (3.22) with the currently available mechanical solutions is hardly achievable.

3.5.2 Euler-Lagrange method based formalization of the dynamics

In order to be able to accurately model the system, an energy based method will be used. The Euler-Lagrange method gives the equation of motion of the system, by using only the potential and kinetic energy. For brevity, we assume that the formulas of the instantanous positions $(P_0(t) - P_2(t))$ of the robot are given. For the sake of completeness, the ommited formulas are given in the Appendix.

The potential energy of the system can be formulated by the following way

$$U = g(m_1 y_{CM1} + m_2 y_{CM2}). \tag{3.25}$$

The kinetic energy, by neglecting the angular momentum, can be written by

$$K = \frac{1}{2}m_1(\dot{P}_{CM1})^2 + \frac{1}{2}m_2(\dot{P}_{CM2})^2. \tag{3.26}$$

Now, the Lagrangian of the system is defined as $L = K - U$, which will be used to formulate the Euler-Lagrange equation

$$\frac{\mathrm{d}}{\mathrm{d}t}\left(\frac{\partial L}{\partial \dot{Q}}\right) - \frac{\partial L}{\partial Q} = 0, \tag{3.27}$$

where $Q = [q_1 \ q_2] = [\theta \ y_0]$. (3.27) also called the equation of motion (EOM) which can be written in the form of state space equation

$$u = M(Q)\ddot{Q} + V(Q,\dot{Q})\dot{Q} + G(Q), \tag{3.28}$$

where u is the total input torque or force and the M is the mass matrix

$$M = \begin{bmatrix} \frac{1}{4}\left(m_1 l_{C1}^2 + (l^2 + 2\cos(q_1) l_{C2}l + l_{C2}^2) m_2\right) & \frac{1}{2}\cos\left(\frac{q_1}{2}\right)(l_{C1}m_1 + (l + l_{C2}) m_2) \\ \frac{1}{2}\cos\left(\frac{q_1}{2}\right)(l_{C1}m_1 + (l + l_{C2}) m_2) & m_1 + m_2 \end{bmatrix},$$

V is the Coriolis and centrifugal matrix

$$V = \begin{bmatrix} -\frac{1}{4}l\sin(q_1) l_{CM2}m_2\dot{q}_1 & 0 \\ -\frac{1}{4}\sin\left(\frac{q_1}{2}\right)(l_{CM1}m_1 + (l + l_{CM2}) m_2)\dot{q}_1 & 0 \end{bmatrix},$$

and G is a vector, with terms responsible for the contribution of the gravity

3. A NOVEL CONCEPT: THE EMULATED ELASTIC ACTUATOR

$$G = \begin{bmatrix} \frac{1}{2}g\cos\left(\frac{q_1}{2}\right)\left(l_{\text{CM1}}m_1 + \left(l + l_{\text{CM2}}\right)m_2\right) \\ g\left(m_1 + m_2\right) \end{bmatrix}.$$

The first row of the equation corresponds to the first degree-of-freedom, namely the knee joint, and the second row is to the second DOF, respectively.

Considering the fact that the system is underactuated, $u = [\tau_\theta \ 0]^T$ where τ_θ is the torque applied on the knee joint. The reason for the second row of u is being zero, is because we have no direct control over the second degree-of-freedom.

In our particular case u must be modified in order to include the external forces acting on the system. The first one is the ground reaction force (GRF) appears when the robot is in contact with the ground

$$F_{GRF} = \frac{k_{GRF}}{1 + e^{100y_0}}, \tag{3.29}$$

where the ground contact is modeled as a linear spring with k_{GRF} constant that sets the stiffness. This is necessary to prevent the model to collapse.

The second one is the friction acts on the mechanism, where only viscous type are assumed

$$\tau_f = B_f\dot{\theta}, \tag{3.30}$$

Based on these, the modified u' generalized input vector takes the form of

$$u' = u + \begin{bmatrix} \tau_f \\ F_{GRF} \end{bmatrix}. \tag{3.31}$$

Now we have formulated the system dynamics, finally the last step is to come up again with an appropriate I_{ref} to realize the desired non-linear behaviour (3.22). In order to be able to realize arbitrary spring functions, the method of the look up table (LUT) is used. The global control precalculates the desired function and with a given discretization is space (in terms of angle $0.01°$ is used) it transmits to the EEA that stores at its LUT.

3.5.3 Simulation and experimental result

In order to be able to realize the proposed model in hardware, the problem of the vertical axis constraint first must be addressed. A lightweight, low-friction mechanism is required to keep the robot move along the vertical axis. I designed and implemented a custom aluminum mechanism with ball-bearings that can be seen in Fig. 3.18.

It weighs only 45 gramms each of those and features very low level of friction. I also designed a custom wire transmission with gear ratio of 4:1. It has zero backlash and almost zero friction. As already pointed out in the Introduction, these mechanical properties are required to be able to successfully implement the concept of the Emulated Elastic Actuator.

For this particular robot, the leg length is $l = 0.17$ m, the weight of the lower link is $m_1 = 0.08$ kg and the upper link is $m_2 = 0.52$ kg. This is accordance with the assumption on page 59.

A similar simulation, like in Section 3.4, was done by numerically computing the system dynamics that was formulated in the previous section. The value of the k_{ns} was -108 and the θ_r was set to $110°$. The initial conditions were $\theta = \theta_r$, $\dot{\theta} = 0$
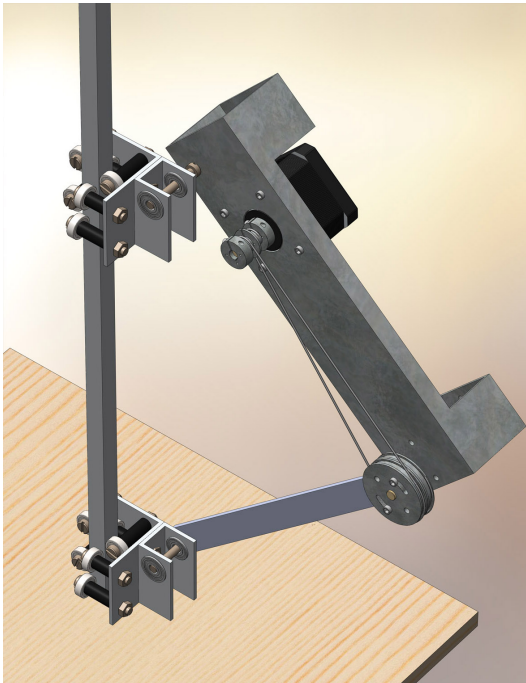
(a) Preliminary CAD design   (b) Real implementation
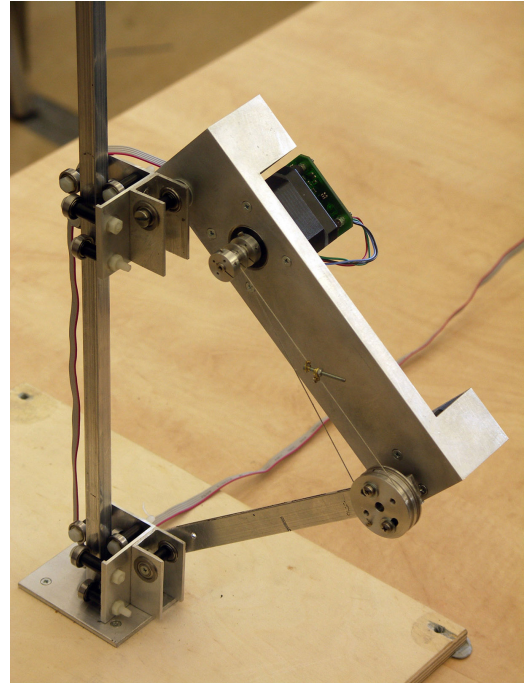
Figure 3.18: One legged robot with two degree-of-freedom.

3. A NOVEL CONCEPT: THE EMULATED ELASTIC ACTUATOR

and $y_0 = 0$. The expected result of the simulation is a clear harmonic oscillation, regarding of the height of the hip (y_2) over time. The result of the simulation can be followed in Fig. 3.19 where height is measured in mm.

In order to verify the simulation result, the same elastic behavior was programmed through a 1800-element LUT in the EEA. With the same initial conditions the expected result would be the same, but a slightly more damped signal was measured (Fig. 3.19). The possible reason for this small difference is the unmodeled friction of the constraining mechanism. Despite the small modeling error, the system behaves as it is expected, namely shows a harmonic oscillation.
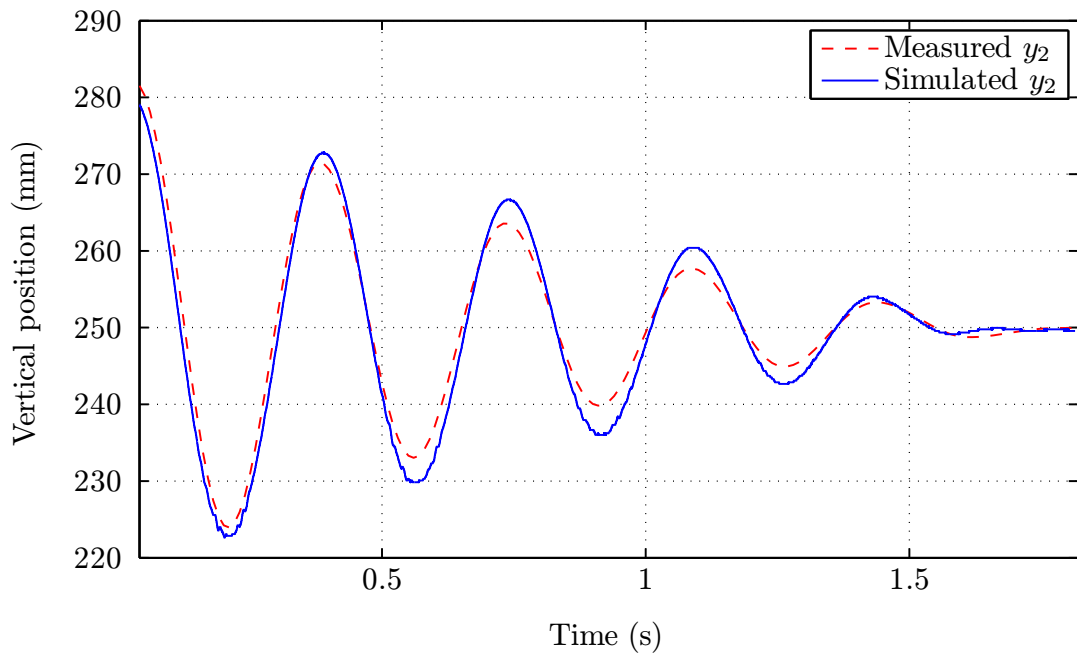
Figure 3.19: Simulation and experimental result of the non-linear elastic behavior that realize the linear virtual spring

In the light of the results, we can conclude that the concept of the emulated elastic actuator can be also used to implement non-linear elastic behavior.

Finally, in the last section, the limitations of the concept will be investigated.

65

3.6 Analysis of the limiting factors

In this section, the detailed analysis of the emulation's limiting factors will be covered. The prescending sections showed that the concept of the emulated elasticity found to be able to efficently mimic the behavior of a physical spring. Limiting factors, like current limitation and torque saturation, were ignored. However, obviously, these questioned must be answered. Hence, limitations in terms of position, speed, acceleration and torque will be presented.

3.6.1 Position

The most important feedback of the system is the position of the motor's shaft. Commonly, rotational encoders are used to measure the angle of the shafts. In my case, magnetic type rotational encoder is used, but the following can be generalized for any type of sensor. First of all, the error of the sensor can be spatial or temporal.

Spatial inaccuracy mainly originate from the inherent non-linearity of the sensor, from the internal or external noise, and from the coarse spatial resolution. The latter one, in case of optical encoders, gain up to 20 or more bits which means 1.24 arcsec or less. In addition, due to the operational principle of the optical encoders the sensor noise is negligible. Non-lineartity, which comes from the fabrication inaccuracy, is typically well below 1%. In case of my magnetic encoder, the resolution is 15-bit that yields to 39.6 arcsec as the finest angle deviation that can be distinguished. Due to the principle of magnetic encoders, external magnetic field can slightly interfere with the measurement but in a good design internal noise dominates. By low-pass filtering the signal noise level of 0.5 LSB is achievable. Due to the common misalignment of the magnet, non-linearity is between 1-2%. It is a good engineering practice to calibrate the magnet within the completed design to improve the non-linearity error. Let's denote by θ_Δ the finest angle increment that the sensor is capable to measure. As already pointed out in Section 3.2, electronic commutation of the motor is based on the angle of the motor's shaft. The relationship is sinusoidal, therefore θ_Δ specifies how coarse or how fine the commutation will be. Fig. 3.20 shows the approximation of a sinusoid based on a 11-bit ($\theta_\Delta = 10.55$ arcmin) and a 15-bit ($\theta_\Delta = 39.6$ arcsec) sensor. As it can be seen, even 15-bit spatial resolution gives acceptable result, further increase is not necessary.

Temporal inaccuracy mainly originate from the delay caused by the low-pass filtering of the signal, and from the delay of the processing and the read out. In

3. A NOVEL CONCEPT: THE EMULATED ELASTIC ACTUATOR
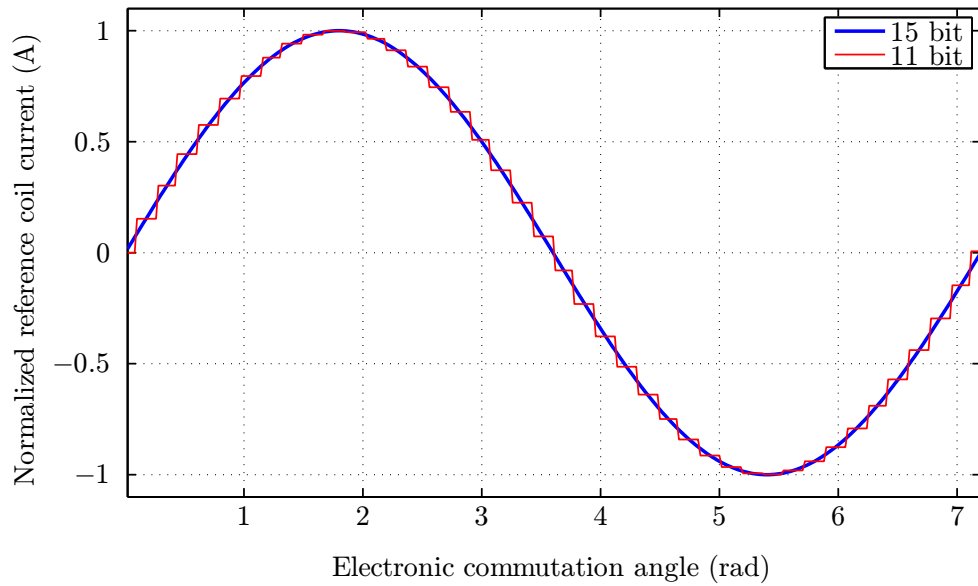
Figure 3.20: Positional accuracy of a 11 vs 15-bit sensor.

case of the industry standard optical encoder, signal conditioning is minor compared to the read out time that is in the range of 1-10μs. Magnetic sensors need notable filtering. In the case of our sensor with normal level of low-pass filtering, that reduces the noise level to 1 LSB, 120 μs of delay is introduced. The signal with the lowest level of filtering, containing 2.5 LSB of noise, means 60 μs delay. The typical read out time adds additial 5μs. According to this, a minimum of 65 μs delay is introduced that has significant influence on the maximum speed and acceleration. Linear prediction can help to reduce the positional error caused by the delay, but limited to motions with constant angular rate since accurate acceleration measurement is not possible in most of the cases.

Taken together, from the emulation point of view there is no significant limitation regarding position.

3.6.2 Speed

In terms of speed measurement, the commonly used methods are limited to differentiating the signal of the position sensor in time. The result is noisy and therefore needs filtering. It is a common approach to use digital filtering (FIR) to smooth the signal that introduces delay. This is why high resolution encoders are used, since at a given shaft speed and sample time the higher the resolution the higher the differential is.

67

3.   A NOVEL CONCEPT: THE EMULATED ELASTIC ACTUATOR

In terms of achievable shaft speed, there are important limitations regarding of commutation latency and available supply voltage. Both are due to the torque limitation that is caused by the increasing speed. First, analyse the effect of the commutation latency on the shaft speed. Let ω_m be an arbitrary angular speed of the motor's shaft and Δt_L is the total latency in the commutation. Then the positional difference caused by Δt_L is

$$\Delta\theta_L = N\omega_m\Delta t_L. \tag{3.32}$$

Taken the equation of the instantaneous motor torque (3.4) and substituting the two reference phase current (3.10)–(3.11) that is been compensated with the delay yields to

$$\begin{aligned} \tau'_m &= K_T I_{ref}\left[\sin(\theta_e)\sin(\theta_e+\Delta\theta_L)+\cos(\theta_e)\cos(\theta_e+\Delta\theta_L)\right] = \\ &= K_T I_{ref}\cos(\Delta\theta_L). \end{aligned} \tag{3.33}$$

This inherently implies that the torque loss due to the latency in the commutation takes the form of

$$\tau_{loss} = 1 - \cos(\Delta\theta_L). \tag{3.34}$$

For a given ($\omega_m = 25$ rad/s) angular speed the loss in percentage is plotted in Fig. 3.21. This indicate that at reaching total latency of 1.25 ms the motor prevented to accelerate. In our particular case, the sum of the sensor, processing and current setting delay is less then 150 μs that corresponds to only 1.8% loss
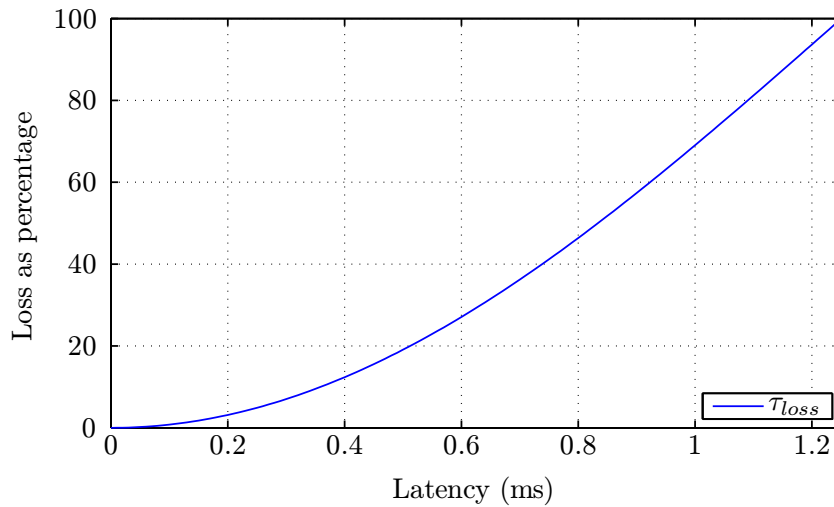
Figure 3.21: Percentage of the loss in torque versus commutation latency.

3. A NOVEL CONCEPT: THE EMULATED ELASTIC ACTUATOR

in torque. According to this, commutation latency must be kept low in order to prevent significant degradation in the available torque at high speed.

In terms of supply voltage, a more significant limitation appears as we decrease the motor voltage. As already pointed out, transconductance type of driver is needed to control the currents of the two phases. However, as current increases and the motor reaches higher speeds, the voltage drop on R (V_R) and the counter-electromotive force (V_{BEMF}) tends to reduce the voltage available to set the desired level of current. The equivalent circuit was presented in Fig. 3.5. By introducing a new voltage source (V) as the sum of the supply voltage and the counter-electromotive force, the Laplace transform of the current $i(t)$ becomes

$$I(s) = \frac{V}{s} \frac{1}{R + Ls},\tag{3.35}$$

from which the Inverse Laplace transform gives the required current in time domain

$$i(t) = \frac{V}{R} \left(1 - \frac{e^{-\frac{R}{L}t}}{R} \right).\tag{3.36}$$

According to this, the time constant of the system is $\tau = \frac{L}{R}$, which tells how long it takes to reach the 63% of the maximum current ($\frac{V}{R}$). From (3.36) one can see that in order to reach faster a given level of current, a higher voltage is needed. Once the required current is reached the voltage must be switched off to prevent the current to go beyond. Fig. 3.22 shows the current settling versus time. V_1 is the voltage
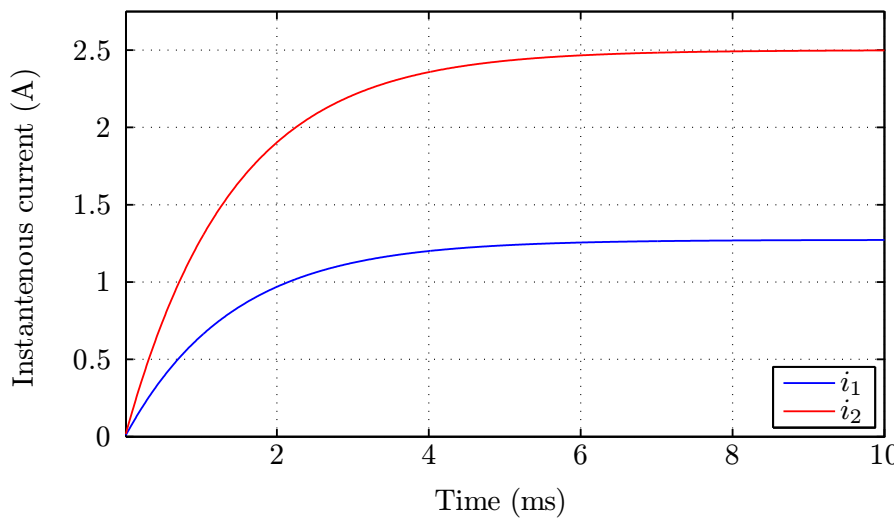
Figure 3.22: Current settling over the two supply voltages (V_1=6.11V and V_2=12V)

required to reach the rated current of the motor, and V_2 is two times higher. As it can be seen, the higher voltage forces a steeper current rise, but exceeds the desired current, therefore needs active control to maintain it. This is how the motor driver tries to keep the current at the reference level. In order to explicitly formulate for a given motor and voltage supply that how long is it possible to do that, we must take the worst case into account. For a given sinusoidal current the highest slope is at zero crossing. According to this, by applying Kirchhoff's voltage law one can write

$$V_A = K_T\omega + I_{rated}R + NI_{rated}\omega L, \tag{3.37}$$

and the same equation could be formulated for V_B so lower index is ommited. Now, if we solve for ω we end up with

$$\omega = \frac{V + I_{rated}R}{K_T + I_{rated}LN}. \tag{3.38}$$

From this equation, one can tell what is the maximum angular speed that is available for a given motor and supply voltage. For example, in the case of our motor, the maximum available speed applying voltage level from 1V to 22V is depicted in Fig. 3.23. This is accordance with (3.36) since at least 6.11V is required to reach the rated current, and after that point the speed shows linear relationship with the applied voltage.

In contrast, if we would like to see how the magnitude of the current effects the maximum achievable angular speed, we find non-linear relation. As we decrease
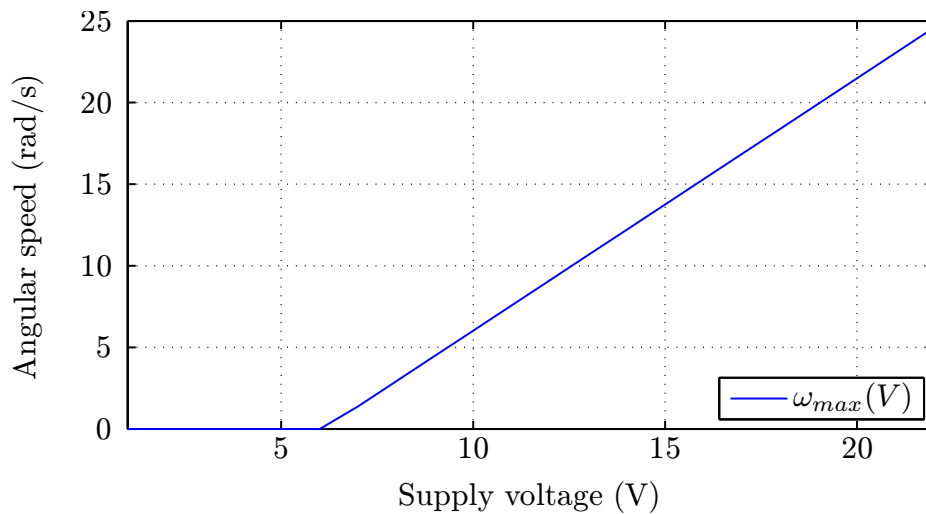
Figure 3.23: Maximum available angular speed as a function of the supply voltage.

the current from the maximum (rated), V_R and V_L voltage drop tends to be zero. Fig. 3.24 illustrates this non-linear relationship. Please remark that, according to
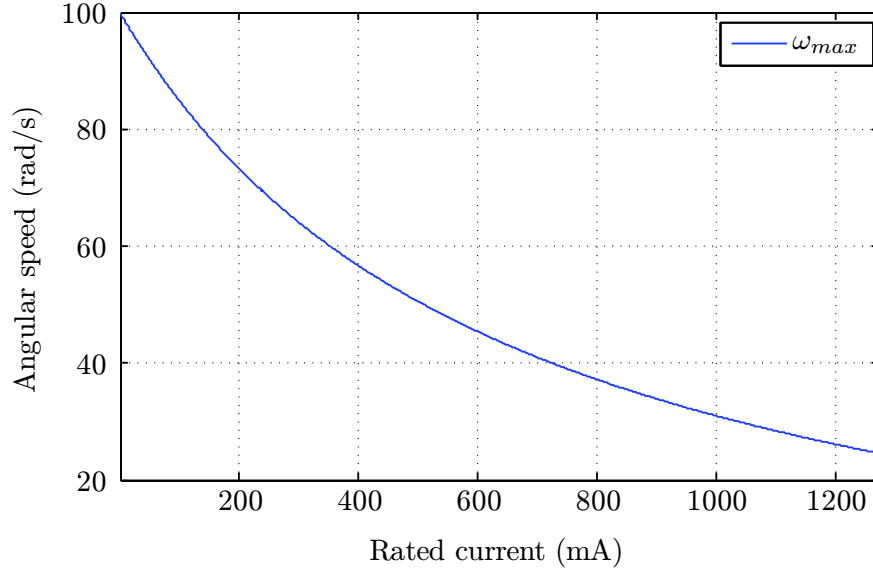
Figure 3.24: Maximum available angular speed versus the magnitude of the current.

the torque drop due to the latency (3.34) high-speed operation with low current level can be limited. In our particular case, at the maximum rated current, angular speed of 25 rad/s can be attained from supply voltage of 22V.

We can conclude that, commutation latency has minor impact on maximum angular speed, but care must be taken to avoid torque losses. The available supply voltage has more significant contribution to the decrease in the maximum speed. For high-speed operation 36V or 48V supply is recommended.

3.6.3 Acceleration

In terms of acceleration measurement, it is not an engineering practice to differentiate again the speed signal in time. The reason for that, the speed is already a noisy signal and the filtering would introduce unacceptable level of delay.

At a given motor torque(τ_m) the instantenous angular acceleration (α) follows Newton's second law

$$\alpha = \frac{\tau}{J}, \tag{3.39}$$

where J is the mass moment of inertia. In order to maximaize acceleration the inertia of the system must be kept low.

Chapter 4

Summary

4.1 Main findings and results

In this dissertation, various solutions have been proposed to improve the present and future actuators of walking robots. Firstly, it has been demonstrated that the non-linearity of the transmissions, caused by the backlash of the gears, can considerably be improved by applying two antagonistic Permanent Magnet Stepper Motors in a flexor-extensor configuration that are supervised by the proposed low-level algorithm. Secondly, the author presented a novel concept of a fully electric actuator that was proven to be capable of emulating various elastic behaviour under software control, furthermore the creation of a robotic joint with up to real-time reconfigurable non-linear elasticity.

4.2 New scientific results

I. Thesis group: Bio-inspired solution for a non-linear phenomenon of low-cost robotic actuators.

Most robotic joints are actuated by rotational mechanisms. Typically, these mechanisms are driven by electric motors whose operating speed is higher than what the joints actually require. Therefore gearboxes are used to reduce the speed of the joints and also to increase their torque capability. The incorporation of a gearbox corrupts the continuity of the torque transmission in most cases because of the backlash phenomenon. Backlash originates from the gear play that results from the imperfectness of the fabrication or the increased wear level of the mating gears. During static motion this introduces only positioning errors but in dynamic cases limit-cycles may occur. My approach was to use a pair of low-cost actuators instead of a more expensive solution that contains a harmonic drive. Then one actuator is dedicated for the right turn and the other for the left turn like the flexing and extending in the human limbs. A smooth motion could be realized with a proper control by mimicking a simple reciprocal innervation of the two muscle groups.

I.1. I designed and implemented a PMSM based low-cost robotic joint that was inspired by the human flexor-extensor mechanism. I proposed a low-level algorithm that was proved to reduce the level of backlash by 90%.

In addition, to support the applicability of the technique we have successfully

enhanced our previously build 11 DOF biped robot [3] to reduce the significant backlash of the joints.

II. Thesis group: The novel concept of the Emulated Elastic Actuator.

The classical robotics requires the transmission between the actuator and the load to be very stiff. But in the last decade the tradition of "the stiffer the better" seems to be changed. Nowadays compliant actuator designs are gaining increasing popularity. One of the reason for that design is to overcome the limitations of a rigid transmission in terms of shock survivability, force control stability and human-safe operation. In the light of the foregoing, I proposed a new concept of fully electric emulation of joint elasticity for biped robots and for other applications (patent pending). I called it the Emulated Elastic Actuator after the Series Elastic Actuator. The idea was to come up with a mechanism that has very low gear ratio, that is highly backdrivable, and has practically zero backlash and then use an electric motor, with a high-speed local control, to produce the required torque in every time instance to mimic the behaviour of a physical spring.

II.1. I proposed the concept of a novel fully electronic actuator that, in contrast to the Series Elastic Actuator used in the state-of-the-art dynamic walking robots, creates physical elasticity under local high-speed software control without the need of springs.

With the help of the EEA concept, I have investigated two linear elastic behaviour. I have implemented the simple Hookean and the Kelvin-Voight models with different elasticity parameters. I have run numerical simulations including the detailed stepper motor dynamics. For validating the simulation results real hardware implementation was used to provide experimental measurements.

II.2. By using the Hookean and the Kelvin-Voight elasticity model I have shown that the concept of the EEA can be used to mimic the behavior of a physical spring with linear characteristics. I also showed the feasibility of emulating positive or even negative damping.

It is a common approach to model our legs as springs [50, 51]. During touchdown, the compression of the virtual spring imitates the behavior of the leg as it is trying to absorb the impact. Apparently, not only the human legs can be modeled as springs but the biped robot's as well. In order to realize even a simple linear

virtual spring, non-linear elastic behavior is required at the joints, however, state-of-the-art compliant actuators are usually limited to linear elasticity. In order to investigate the emulation of non-linear springs, I designed and implemented an underactuated, one legged robot with two degree of freedom. Euler-Lagrange method was used to formulate the dynamics of the system, that was used to run the numerical simulation. Hardware realization was used to validate the theoretical result.

II.3. I extended the concept of the Emulated Elastic Actuator to non-linear elastic behavior. By constructing and modelling, with the Euler-Lagrange method, an underactuated one-legged robot I have demonstrated that, contrary to state-of-the-art compliant actuators, reconfigurable elasticity with non-linear characteristic can be efficiently realized with the EEA.

And finally, the practicle limitations of the Emulated Elastic Actuator has been analyzed in terms of position, speed, and acceleration.

4.3 Application of the results

During my work, all the algorithms and hardware realizations I made give a possible solution for real and up to date problems.

The results of the first thesis group offer a solution for creating high degree-of-freedom low-cost robotic joints with a reduced level of backlash. For example, for humanoid robots with 30 or more DOFs the result could be used to eliminate the need for expensive harmonic drives. Therefore, the proposed solution is highly recommended for moderate cost humanoid or other legged robotic applications.

In terms of the second thesis group, the main application of the results would be legged robots. A new type of actuator is presented that could be a promising alternative of the Series Elastic Actuators. The novel actuator can be useful almost in any case where SEA is used. For example, in walking, hopping and running robots. Incorporating the EEA with humanoid robots could lead to an even better human-like motion.

In addition, the EEA could also be used in modern manipulators that extends the possible applications to industrial utilization. Industrial manipulators can be improved by further enhancing the safety of the co-working with humans. Additional applications could be found in the field of industry that could utilize the

4. SUMMARY

ability of the concept of mimicking elastic behavior. For example, in the service industry or in the automobile industry knobs with reprogrammable torque-deflection characteristic would be achievable (like the BMW iDrive, etc.).

Journal Publications of the Author

[1] B. G. Soós, Á. Rák, **J. Veres**, and G. Cserey, "GPU boosted CNN simulator library for graphical Flow-Based programmability," *EURASIP Journal on Advances in Signal Processing*, vol. 2009, pp. 1–12, 2009.

[2] **J. Veres**, G. Cserey, and G. Szederkényi, "Bio-inspired backlash reduction of a low-cost robotic joint using closed-loop-commutated stepper motors," *Robotica*, vol. FirstView, pp. 1–8, 4 2013.

International Conference Publications of the Author

[3] Á. Tar, **J. Veres**, and G. Cserey, "Design and realization of a biped robot using stepper motor driven joints," in *Mechatronics, 2006 IEEE International Conference on*, pp. 493–498, 2006.

[4] B. G. Soós, Á. Rák, **J. Veres**, and G. Cserey, "GPU powered CNN simulator (SIMCNN) with graphical flow based programmability," in *2008 11th International Workshop on Cellular Neural Networks and Their Applications*, (Santiago de Composteia, Spain), pp. 163–168, 2008.

[5] N. Hóz, **J. Veres**, and G. Cserey, "Hall position encoder-based touch surface," in *2011 IEEE/ASME International Conference on Advanced Intelligent Mechatronics (AIM)*, pp. 220–225, IEEE, July 2011.

[6] N. Sarkány, G. Cserey, Á. Tar, and **J. Veres**, "Design of a biomechatronic hand (BMT-H) actuated by the flexor-extensor mechanism," in *2011 IEEE/ASME International Conference on Advanced Intelligent Mechatronics (AIM)*, pp. 446–450, IEEE, July 2011.

Patents of the Author

[7] **J. Veres**, Á. Tar, and G. Cserey, "Hajtómechanizmus." *Hungarian Patent*, No. P1200012/1.

[8] Á. Tar, **J, Veres**, and G. Cserey, "Érzékelő eszköz." *Hungarian Patent*, No. P1100633/1.

References

[1] K. Ichiro, *Development of Waseda Robot.* Humanoid Robotics Institute, Waseda University, 1985.

[2] Y. Sakagami, R. Watanabe, C. Aoyama, S. Matsunaga, N. Higaki, and K. Fujimura, "The intelligent ASIMO: system overview and integration," in *Intelligent Robots and Systems, 2002. IEEE/RSJ International Conference on*, vol. 3, pp. 2478–2483, 2002.

[3] P. Sardain and G. Bessonnet, "Forces acting on a biped robot. center of pressure-zero moment point," *Systems, Man and Cybernetics, Part A: Systems and Humans, IEEE Transactions on*, vol. 34, no. 5, pp. 630–637, 2004.

[4] M. Vukobratovic and B. Borovac, "Zero-moment point-thirty five years of its life," *International Journal of Humanoid Robotics*, vol. 1, no. 1, p. 157â173, 2004.

[5] D. G. Hobbelen and M. Wisse, "Limit cycle walking," *Humanoid Robots, Human-like Machines*, 2007.

[6] E. R. Westervelt, J. W. Grizzle, and C. Chevallereau, *Feedback control of dynamic bipedal robot locomotion.* CRC Press, June 2007.

[7] G. Pratt and M. Williamson, "Series elastic actuators," in *Intelligent Robots and Systems 95. 'Human Robot Interaction and Cooperative Robots', Proceedings. 1995 IEEE/RSJ International Conference on*, vol. 1, pp. 399–406 vol.1, 1995.

[8] S. Villwock and M. Pacas, "Time-Domain identification method for detecting mechanical backlash in electrical drives," *Industrial Electronics, IEEE Transactions on*, vol. 56, no. 2, pp. 568–573, 2009.

[9] M. Ruderman, F. Hoffmann, and T. Bertram, "Modeling and identification of elastic robot joints with hysteresis and backlash," *Industrial Electronics, IEEE Transactions on*, vol. 56, no. 10, pp. 3840–3847, 2009.

[10] M. Lorinc and B. Lantos, "Modeling, identification, and compensation of Stick-Slip friction," *Industrial Electronics, IEEE Transactions on*, vol. 54, no. 1, pp. 511–521, 2007.

[11] S. Villwock and M. Pacas, "Deterministic method for the identification of backlash in the time domain," in *Industrial Electronics, 2006 IEEE International Symposium on*, vol. 4, pp. 3056–3061, 2007.

[12] R. Merzouki, J. Davila, L. Fridman, and J. Cadiou, "Backlash phenomenon observation and identification in electromechanical system," *Control Engineering Practice*, vol. 15, no. 4, pp. 447–457, 2007.

[13] P. Rostalski, T. Besselmann, M. Baric, F. Van Belzen, and M. Morari, "A hybrid approach to modelling, control and state estimation of mechanical systems with backlash," *International Journal of Control*, vol. 80, no. 11, p. 1729, 2007.

[14] S. Villwock and M. Pacas, "Application of the Welch-Method for the identification of two- and Three-Mass-Systems," *Industrial Electronics, IEEE Transactions on*, vol. 55, no. 1, pp. 457–466, 2008.

[15] M. F. Lima, J. A. Machado, and M. Crisostomo, "Experimental backlash study in mechanical manipulators," *Robotica*, vol. 29, no. 02, pp. 211–219, 2011.

[16] N. H. Kim, U. Y. Huh, and J. G. Kim, "Fuzzy position control of motor plant with backlash," in *Industrial Electronics Society, 2004. IECON 2004. 30th Annual Conference of IEEE*, vol. 3, pp. 3190–3195, 2005.

[17] A. Lagerberg and B. Egardt, "Backlash estimation with application to automotive powertrains," *Control Systems Technology, IEEE Transactions on*, vol. 15, no. 3, pp. 483– 493, 2007.

[18] L. Márton and B. Lantos, "Control of mechanical systems with stribeck friction and backlash," *Systems & Control Letters*, vol. 58, no. 2, pp. 141–147, 2009.

[19] L. Márton, "Adaptive friction compensation in the presence of backlash," *Journal of Control Engineering and Applied Informatics*, vol. 11, no. 1, p. 3, 2009.

[20] M. Nordin and P. Gutman, "Controlling mechanical systems with backlash-a survey," *Automatica*, vol. 38, no. 10, pp. 1633–1649, 2002.

[21] R. Kalantari and S. Foomanr, "Backlash nonlinearity modeling and adaptive controller design for an electromechanical power transmission system," *Scientia Iranica Transaction B: Mechanical Engineering*, vol. 16, no. 6, pp. 463–469, 2009.

[22] R. Merzouki and J. Cadiou, "Estimation of backlash phenomenon in the electromechanical actuator," *Control Engineering Practice*, vol. 13, no. 8, pp. 973–983, 2005.

[23] H. Mokhtari and F. Barati, "A new scheme for a mechanical load position control driven by a permanent magnet DC motor and a nonzero backlash gearbox," in *Industrial Electronics, 2006 IEEE International Symposium on*, vol. 3, pp. 2052–2057, 2007.

[24] M. Gruzman, H. I. Weber, and L. L. Menegaldo, "Time domain simulation of a target tracking system with backlash compensation," *Mathematical Problems in Engineering*, p. 27, 2010.

[25] G. E. Hovland, S. Hanssen, E. Gallestey, S. Moberg, T. Brogardh, S. Gunnarsson, and M. Isaksson, "Nonlinear identification of backlash in robot transmissions," in *Proceedings of the 33rd ISR (International Symposium on Robotics)*, 2002.

[26] B. J. Jung, J. S. Kong, B. H. Lee, S. M. Ahn, and J. G. Kim, "Backlash compensation for a humanoid robot using disturbance observer," in *Industrial Electronics Society, 2004. IECON 2004. 30th Annual Conference of IEEE*, vol. 3, pp. 2142–2147, 2005.

[27] J. S. Kong, B. J. Jung, B. H. Lee, and J. G. Kim, "Nonlinear motor control using dual feedback controller," in *Industrial Electronics Society, 2005. IECON 2005. 31st Annual Conference of IEEE*, p. 6, 2006.

[28] A. Akhter and A. Shafie, "Advancement of android from ancient time to present time and contribution of various countries in the research and development of the humanoid platform," *International Journal of Robotics and Automation (IJRA)*, vol. 1, no. 2, p. 42, 2010.

[29] S. G. Robertz, L. Halt, S. Kelkar, K. Nilsson, A. Robertsson, D. Schar, and J. Schiffer, "Precise robot motions using dual motor control," in *Robotics and Automation (ICRA), 2010 IEEE International Conference on*, pp. 5613–5620, 2010.

[30] R. Boudreau, X. Mao, and R. Podhorodeski, "Backlash elimination in parallel manipulators using actuation redundancy," *Robotica*, vol. 1, no. 1, pp. 1–10, 2010.

[31] Y. Ohba, S. Katsura, and K. Ohishi, "Friction free bilateral robot based on twin drive control system considering two resonant frequencies," in *Industrial Electronics Society, 2005. IECON 2005. 31st Annual Conference of IEEE*, p. 6 pp., 2005.

[32] C. Mitsantisuk, K. Ohishi, S. Urushihara, and S. Katsura, "Identification of twin direct-drive motor system with consideration of wire rope tension," in *Mechatronics, 2009. ICM 2009. IEEE International Conference on*, pp. 1–6, 2009.

[33] S. Lyshevski, "Electromechanical flight actuators for advanced flight vehicles," *Aerospace and Electronic Systems, IEEE Transactions on*, vol. 35, no. 2, pp. 511–518, 1999.

[34] K. Tsui, N. Cheung, and K. Yuen, "Novel modeling and damping technique for hybrid stepper motor," *Industrial Electronics, IEEE Transactions on*, vol. 56, no. 1, pp. 202–211, 2009.

[35] P. Crnosija, B. Kuzmanovic, and S. Ajdukovic, "Microcomputer implementation of optimal algorithms for closed-loop control of hybrid stepper motor drives," *Industrial Electronics, IEEE Transactions on*, vol. 47, no. 6, pp. 1319–1325, 2000.

[36] P. Krishnamurthy and F. Khorrami, "An analysis of the effects of Closed-Loop commutation delay on stepper motor control and application to parameter

estimation," *Control Systems Technology, IEEE Transactions on*, vol. 16, no. 1, pp. 70–77, 2008.

[37] A. I. Chirila, I. D. Deaconu, V. Navrapescu, M. Albu, and C. Ghita, "On the model of a hybrid step motor," in *IEEE International Symposium on Industrial Electronics, 2008. ISIE 2008*, pp. 496–501, 2008.

[38] F. Belkhouche and S. Muzdeka, "A linearized model for permanent magnet stepper motors," in *Industrial Electronics Society, 2003. IECON '03. The 29th Annual Conference of the IEEE*, vol. 1, pp. 301–305 vol.1, 2003.

[39] S. Haddadin, A. Albu-Schaffer, and G. Hirzinger, "Safety evaluation of physical human-robot interaction via crash-testing," in *Robotics: science and systems conference (RSS2007)*, pp. 217–224, 2007.

[40] S. Migliore, E. Brown, and S. DeWeerth, "Biologically inspired joint stiffness control," in *Robotics and Automation, 2005. ICRA 2005. Proceedings of the 2005 IEEE International Conference on*, pp. 4508–4513, 2005.

[41] G. Tonietti, R. Schiavi, and A. Bicchi, "Design and control of a variable stiffness actuator for safe and fast physical human/robot interaction," in *Robotics and Automation, 2005. ICRA 2005. Proceedings of the 2005 IEEE International Conference on*, pp. 526–531, 2005.

[42] R. Schiavi, G. Grioli, S. Sen, and A. Bicchi, "VSA-II: a novel prototype of variable stiffness actuator for safe and performing robots interacting with humans," in *Robotics and Automation, 2008. ICRA 2008. IEEE International Conference on*, pp. 2171–2176, 2008.

[43] J. W. Hurst, J. E. Chestnutt, and A. A. Rizzi, "An actuator with mechanically adjustable series compliance," 2004.

[44] R. Van Ham, M. Van Damme, B. Verrelst, B. Vanderborght, and D. Lefeber, "MACCEPA, the mechanically adjustable compliance and controllable equilibrium position actuator: a 3DOF joint with two independent compliances," *International Applied Mechanics*, vol. 43, no. 4, pp. 467–474, 2007.

[45] S. Wolf and G. Hirzinger, "A new variable stiffness design: Matching requirements of the next robot generation," in *Robotics and Automation, 2008. ICRA 2008. IEEE International Conference on*, pp. 1741–1746, 2008.

[46] A. Albu-Schaffer, S. Haddadin, C. Ott, A. Stemmer, T. Wimbock, and G. Hirzinger, "The DLR lightweight robot: design and control concepts for robots in human environments," *Industrial Robot: An International Journal*, vol. 34, no. 5, pp. 376–385, 2007.

[47] K. Radkhah, S. Kurowski, T. Lens, and O. von Stryk, "Compliant robot actuation by feedforward controlled emulated spring stiffness," *Simulation, Modeling, and Programming for Autonomous Robots*, pp. 497–508, 2010.

[48] B. Bigge and I. R. Harvey, "Programmable springs: Developing actuators with programmable compliance for autonomous robots," *Robotics and Autonomous Systems*, vol. 55, no. 9, pp. 728–734, 2007.

[49] M. Bodson, J. Chiasson, R. Novotnak, and R. Rekowski, "High-performance nonlinear feedback control of a permanent magnet stepper motor," *Control Systems Technology, IEEE Transactions on*, vol. 1, no. 1, pp. 5–14, 1993.

[50] Y. Blum, S. Lipfert, and A. Seyfarth, "Effective leg stiffness in running," *Journal of biomechanics*, vol. 42, no. 14, pp. 2400–2405, 2009.

[51] A. Seyfarth, A. Friedrichs, V. Wank, and R. Blickhan, "Dynamics of the long jump," *Journal of Biomechanics*, vol. 32, no. 1259, p. 1267, 1999.

[52] F. Iida, Y. Minekawa, J. Rummel, and A. Seyfarth, "Toward a human-like biped robot with compliant legs," *Robotics and Autonomous Systems*, vol. 57, pp. 139–144, 2009.

[53] F. Iida, J. Rummel, and A. Seyfarth, "Bipedal walking and running with spring-like biarticular muscles," *Journal of Biomechanics*, vol. 41, no. 3, pp. 656–667, 2008.

Appendix

A.1   Bio-inspired low-cost robotic joint with reduced level of backlash

Table 1: List of constants

B_m	$8{\times}10^{-5}\ \frac{\text{N m s}}{\text{rad}}$
J_m	$1.76{\times}10^{-7}\ \text{kg m}^2$
B_g	$1.1{\times}10^{-4}\ \frac{\text{N m s}}{\text{rad}}$
J_g	$0.4{\times}10^{-7}\ \text{kg m}^2$
B_l	$1.05{\times}10^{-1}\ \frac{\text{N m s}}{\text{rad}}$
J_l	$7.5{\times}10^{-4}\ \text{kg m}^2$
K	$1.46{\times}10^6\ \frac{\text{N}}{\text{m}}$
b	$7.8{\times}10^{-4}\ \text{m}$
r_m, r_{g2}	$3.7{\times}10^{-3}\ \text{m}$
r_{g1}, r_l	$3.7{\times}10^{-2}\ \text{m}$

A.2 A novel concept: The Emulated Elastic Actuator

A.2.1 Concept of the Emulated Elastic Actuator
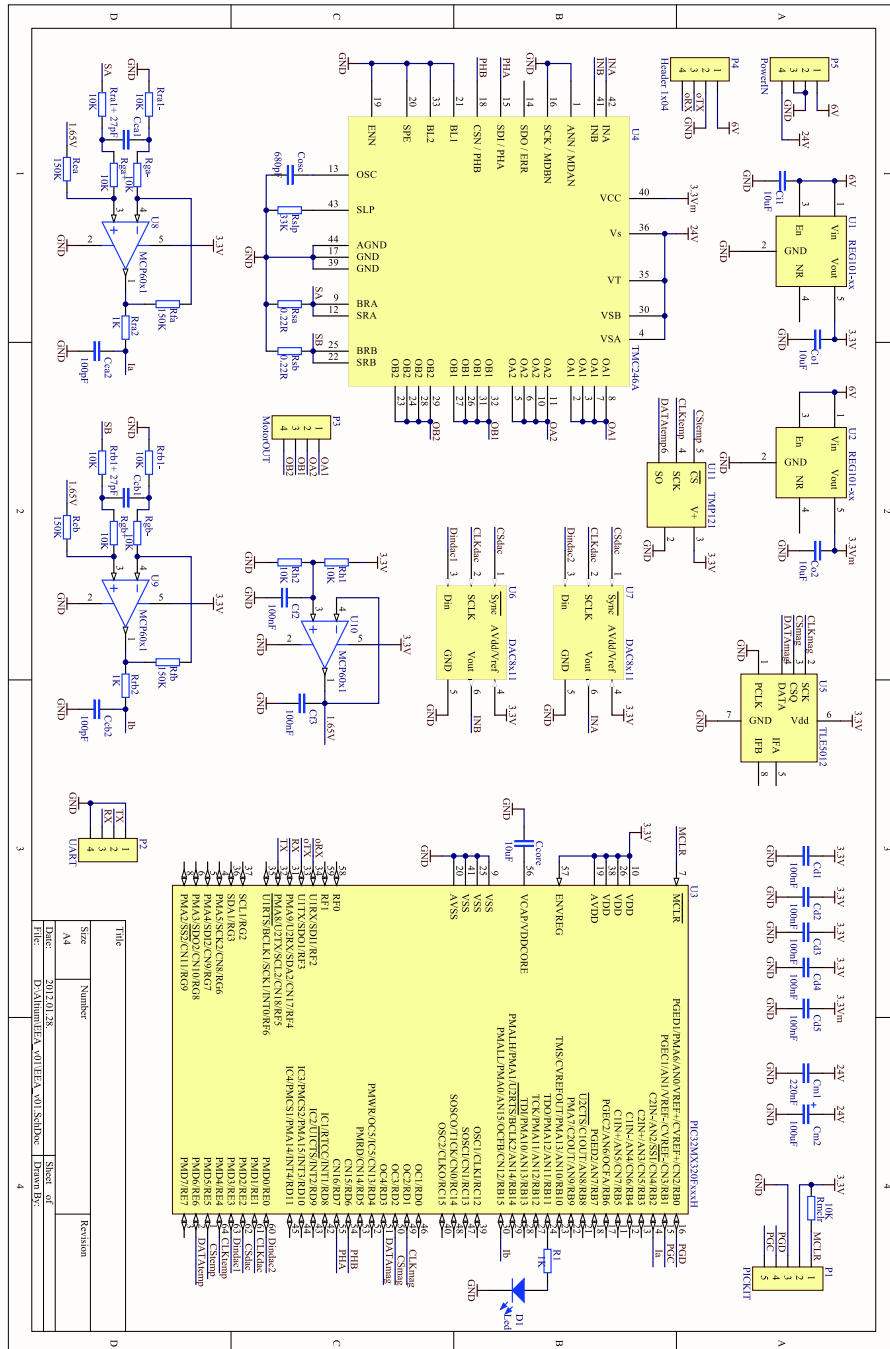
Figure 1: Schematic of the Emulated Elastic Actuator's electronics.

A.2.2 Euler-Lagrange method based formalization of the dynamics

$$P_0 = \begin{pmatrix} 0 \\ q_2 \end{pmatrix}$$

$$P_{CM1} = \begin{pmatrix} \cos\left(\frac{q_1}{2}\right) l_{\text{CM1}} \\ \sin\left(\frac{q_1}{2}\right) l_{\text{CM1}} + q_2 \end{pmatrix}$$

$$P_1 = \begin{pmatrix} l\cos\left(\frac{q_1}{2}\right) \\ l\sin\left(\frac{q_1}{2}\right) + q_2 \end{pmatrix}$$

$$P_{CM2} = \begin{pmatrix} \cos\left(\frac{q_1}{2}\right)(l - l_{\text{CM2}}) \\ l\sin\left(\frac{q_1}{2}\right) + \sin\left(\frac{q_1}{2}\right) l_{\text{CM2}} + q_2 \end{pmatrix}$$

$$P_2 = \begin{pmatrix} 0 \\ 2l\sin\left(\frac{q_1}{2}\right) + q_2 \end{pmatrix}$$

$$\dot{P}_{CM1} = \begin{pmatrix} -\frac{1}{2}\sin\left(\frac{q_1}{2}\right) l_{\text{CM1}}\dot{q}_1 \\ \frac{1}{2}\cos\left(\frac{q_1}{2}\right) l_{\text{CM1}}\dot{q}_1 + \dot{q}_2 \end{pmatrix}$$

$$\dot{P}_{CM2} = \begin{pmatrix} -\frac{1}{2}\sin\left(\frac{q_1}{2}\right)(l - l_{\text{CM2}})\dot{q}_1 \\ \frac{1}{2}\left[\cos\left(\frac{q_1}{2}\right)(l + l_{\text{CM2}})\dot{q}_1 + 2\dot{q}_2\right] \end{pmatrix}$$

$$U = m_1 g\left[\sin\left(\frac{q_1}{2}\right] l_{\text{CM1}} + q_2\right) + m_2 g\left[l\sin\left(\frac{q_1}{2}\right) + \sin\left(\frac{q_1}{2}\right) l_{\text{CM2}} + q_2\right]$$

$$K = \begin{array}{l} \frac{1}{8}\left(m_1\left(l_{\text{CM1}}^2\dot{q}_1^2 + 4\cos\left(\frac{q_1}{2}\right) l_{\text{CM1}}\dot{q}_1\dot{q}_2 + 4\dot{q}_2^2\right) + m_2\left(\sin\left(\frac{q_1}{2}\right)^2(l - l_{\text{CM2}})^2\dot{q}_1^2 + \right. \\ \left. + \left(\cos\left(\frac{q_1}{2}\right)(l + l_{\text{CM2}})\dot{q}_1 + 2\dot{q}_2\right)^2 \end{array}$$

$$EOM = \frac{1}{4}\left(l_{\text{CM1}}^2 m_1\ddot{q}_1 + 2\cos\left(\frac{q_1}{2}\right) l_{\text{CM1}} m_1\left(g + \ddot{q}_2\right) + m_2\left(l_{\text{CM2}}^2\ddot{q}_1 + \right.$$
$$+ \left(l\ddot{q}_1 + 2\cos\left(\frac{q_1}{2}\right)(g + \ddot{q}_2)\right) + l_{\text{CM2}}\left(-l\sin\left(q_1\right)\dot{q}_1^2 + 2\left(l\cos\left(q_1\right)\ddot{q}_1 + \right.$$
$$+ \cos\left(\frac{q_1}{2}\right)(g + \ddot{q}_2)\right), \frac{1}{4}\left(m_1\left(l_{\text{CM1}}\left(-\sin\left(\frac{q_1}{2}\right)\dot{q}_1^2 + 2\cos\left(\frac{q_1}{2}\right)\ddot{q}_1\right) + \right.$$
$$4\left(g + \ddot{q}_2\right) + m_2\left(-\sin\left(\frac{q_1}{2}\right)(l + l_{\text{CM2}})\dot{q}_1^2 + 2\left(\cos\left(\frac{q_1}{2}\right)(l + l_{\text{CM2}})\ddot{q}_1 + 2\left(g + \ddot{q}_2\right)\right)\right)$$